Modulation of Glutathione via ABCC1 and/or System xCT as Antimalarial Chemotherapy

Rachel Xue Ying Shih

Institute of Parasitology

McGill University, Montreal

December 2024

A thesis submitted to McGill University as partial fulfillment of the requirements of the degree of Master of Science

Table of Contents

ABSTRACT

Malaria remains a significant global health challenge, driven by *Plasmodium* parasites and exacerbated by widespread resistance to antimalarial drugs targeting parasitic metabolism. This study explores an alternative strategy by targeting erythrocytes—the host cells where parasites reside—specifically focusing on glutathione (GSH), a key antioxidant essential for maintaining cellular redox homeostasis. We hypothesize that depleting GSH through sulfasalazine (SSZ), which inhibits system xc^-, and apigenin (API), which enhances GSH efflux via ABCC1/MRP1, induces oxidative stress in erythrocytes, selectively eliminating infected cells. Erythrocytes were treated with varying concentrations of API and SSZ, individually and in combination. Reactive oxygen species (ROS) levels were quantified using $DCFH_2$-DA fluorescence, and hemolysis was assessed by measuring optical density at 650 nm. The effects on the proliferation of chloroquine (CQ)-sensitive (3D7) and CQ-resistant (Dd2) *Plasmodium falciparum* strains were evaluated using a SYBR Green I®-based assay. Both API and SSZ significantly increased ROS levels in a dose-dependent manner while causing minimal hemolysis at therapeutic concentrations. They also successfully inhibited parasite proliferation. Although combination therapy enhanced ROS generation, it did not significantly reduce the IC_{50} values for parasite inhibition. Nonetheless, our findings demonstrate that targeting host antioxidative systems with API and SSZ disrupts redox balance in infected erythrocytes, offering a novel strategy to combat malaria while sparing uninfected cells.

RÉSUMÉ

Le paludisme reste un problème de santé mondial important, causé par les parasites *Plasmodium*, et exacerbé par la résistances aux médicaments antipaludiques ciblant leur métabolisme. Cette étude explore une stratégie alternative qui consiste à agir spécifiquement sur le glutathion (GSH), un antioxydant essentiel au maintien de l'homéostasie redox cellulaire, et à cibler les érythrocytes, où siègent les parasites. Nous émettons l'hypothèse que l'épuisement du GSH induit par la sulfasalazine (SSZ), qui inhibe le système xc-, et par l'apigénine (API), qui augmente l'efflux de GSH via ABCC1/MRP1, provoque un stress oxydatif dans les érythrocytes et élimine sélectivement les cellules infectées. Les érythrocytes ont été traités avec des concentrations variables d'API et de SSZ, individuellement et en combinaison. Les niveaux d'espèces réactives de l'oxygène (ROS) ont été quantifiés par fluorescence avec le $DCFH_2$-DA, et l'hémolyse a été évaluée par mesure de la densité optique à 650 nm. Les effets sur la prolifération des souches de *Plasmodium falciparum* sensibles (3D7) et résistantes (Dd2) à la chloroquine ont été évalués à l'aide d'un test basé sur le SYBR Green I®. L'API et le SSZ ont tous deux augmenté de manière significative les niveaux de ROS à dose croissante, tout en provoquant une hémolyse minimale aux concentrations thérapeutiques. Ils ont également réussi à inhiber la prolifération du parasite. Bien que la thérapie combinée ait augmenté la production de ROS, elle n'a pas réduit de manière significative les valeurs IC_{50} pour l'inhibition du parasite. Néanmoins, nos résultats montrent que cibler les systèmes antioxydants des hôtes avec l'API et la SSZ perturbe l'équilibre redox dans les érythrocytes infectés, offrant une stratégie novatrice pour lutter contre le paludisme tout en épargnant les cellules non infectées.

ACKNOWLEDGEMENTS

I would like to express my gratitude to my supervisor, Dr. Elias Georges, for his guidance and support throughout the challenges and triumphs of my research project. My sincere thanks also go to Dr. Momar Ndao, a member of my Research Advisory Committee, for his invaluable advice and for inspiring new research ideas. I am deeply grateful to Dr. Jeffrey Agyapong, Dr. Tosin Opadokun, and Dr. Petra Rohrbach for their tremendous support in enriching my learning and advancing my research.

I wish to express my deepest appreciation to Dr. Daoudi Mohamed, whose assistance in troubleshooting experiments, lending of a helping hand, and heartwarming advice provided strength during difficult times. I am equally thankful to Peter Lee, the facility manager at the Institute of Parasitology, for his exceptional technical support and motivational encouragement. My gratitude also goes to my friends at the Institute of Parasitology, who offered their support, comfort, and laughter, even during my most trying moments.

I am eternally thankful for the love and support of my family, particularly my sister, and my best friend, whose constant encouragement kept me motivated during the pursuit of my Master's degree. Their belief in me was a continual source of strength and inspiration.

Above all, I give my deepest gratitude to Jesus. In moments of solitude and anxiety, you were my refuge, my comfort, and my anchor. Your presence gave me the courage to face my fears and the peace to carry on, even when the path seemed impossible.

Rachel Xue Ying Shih

LIST OF FIGURES

LIST OF ABBREVIATIONS

3D7: chloroquine-sensitive *Plasmodium falciparum*

5-ASA: 5-aminosalicylic acid

ABC: ATP-binding Cassette

ACT: artemisinin-based combination therapies

API: apigenin

ATP: Adenosine triphosphate

Cat: catalase

CD: cluster of differentiation

CDC: Centers for Disease Control and Prevention

COX-2: cyclooxygenase

CPG: carboxyphenylglycine

CPM: complete parasite medium

CQ: chloroquine

DAMP: damage-associated molecular patterns

DCFH2-DA: 2′,7′-Dichlorodihydrofluorescein diacetate

Dd2: chloroquine-resistant *Plasmodium falciparum*

DDT: Dichlorodiphenyltrichloroethane

DHFR: dihydrofolate reductase

DHPS: dihydropteroate synthase

DMSO: Dimethyl sulfoxide

DNA: Deoxyribonucleic acid

DV: digestive vacuole

ELISA: enzyme-linked immunosorbent assay

FDA: United States Food and Drug Administration

G6PD: glucose-6-phosphate dehydrogenase

GCL: glutamate cysteine ligase

GPI: glycosylphosphatidylinositols

GPx: glutathione peroxidase

GR: glutathione reductase

Grx: Glutaredoxin

GSH: glutathione

GSSG: oxidized glutathione

Hb: hemoglobin

HRP-2: Histidine-Rich Protein-2

IBD: inflammatory bowel disease

IC50: half-maximal inhibitory concentration

ICAM-1: Intercellular Adhesion Molecule 1

IL-1β: Interleukin-1beta

IPT: intermittent preventive treatment

IRS: indoor residual spraying

ITN: Insecticide-treated nets

LDH: Lactate dehydrogenase

LOX: lipoxygenase

MDA: mass drug administration

MRP: multidrug resistance-associated protein

NADPH: Nicotinamide adenine dinucleotide phosphate

NBD: nucleotide-binding domain

NO: nitric oxide

NOS: nitric oxide synthase

OD: optical density

PAMP: pathogen-associated molecular pattern

PCR: polymerase chain reaction

PfCRT: *Plasmodium falciparum* Chloroquine Resistance Transporter

PfHRP: *Plasmodium falciparum* histidine-rich protein (PfHRP)

PfEMP1: *Plasmodium falciparum* erythrocyte membrane protein 1

PfMDR1: *Plasmodium falciparum* Multidrug Resistant Protein 1

PPP: pentose phosphate pathway

Prx: peroxidase

RBC: red blood cell

RDT: rapid diagnostic test

ROS: reactive oxygen species

SCD: sickle cell disease

SOD: Superoxide dismutase

SMC: seasonal malaria chemoprevention

SLC: solute carrier

SSZ: sulfasalazine

Sxc−: cystine/glutamate antiporter system xc−

TMD: transmembrane domains

TNF: Tumor necrosis factor

TR: thioredoxin reductase

Trx: thioredoxin

UPR: unfolded protein response

XO: xanthine oxidase

WHO: Wolrd Health Organization

1 INTRODUCTION AND LITERATURE REVIEW

1.1 Malaria

1.1.1 History of Malaria Infection in Humans

Malaria has profoundly shaped human history, with ancient records of malaria-like fevers from China, Egypt, India, and Mesopotamia [1]. Hippocrates linked the disease to swampy areas in the 4th century BC, inspiring its name, "malaria" (bad air) [1]. It weakened the Roman Empire, decimated Crusaders, and thwarted Genghis Khan's conquests [2-3]. European colonization introduced malaria to the New World, influencing the transatlantic slave trade due to African genetic resistance [3]. Quinine, derived from South America's cinchona bark, became the first effective treatment in the 17th century, though its bitterness limited its use until the British Navy popularized "gin and tonic" [4]. Despite this, malaria caused massive casualties during the American Civil War and World War I [2]. World War II marked major progress with antimalarial drug CQ, insecticide DDT, and the formation of the US Malaria Control in War Areas program, now the Centers for Disease Control and Prevention (CDC) [1].

1.1.2 Malaria Prevalence and Distribution

Malaria remains a critical public health challenge despite a decline in incidence from 81.0 per 1,000 at-risk individuals in 2000 to 58.4 in 2022 [5]. According to the World Health Organization (WHO), in 2022, 249 million cases and 608,000 deaths were reported across 85 endemic countries (see Figure 1.), with 93.6% of cases and 95.4% of deaths in the African

Region, where children under five comprised 78.1% of fatalities [5]. Beyond Africa, the Eastern Mediterranean Region reported 8.3 million cases, led by Sudan (41%), with Pakistan seeing 2.1 million cases following severe floods [5]. The Southeast Asia Region reported 5.2 million cases, mostly from India (65.7%), with Myanmar experiencing a sevenfold surge due to political instability [5]. The Western Pacific Region recorded 1.9 million cases, with 90% in Papua New Guinea [5]. The Americas reported 550,000 cases, largely in Venezuela, Brazil, and Colombia [5]. Challenges, including the COVID-19 pandemic and socio-political instability, have disrupted malaria control services, further complicating efforts to reduce the global burden of the disease [5].

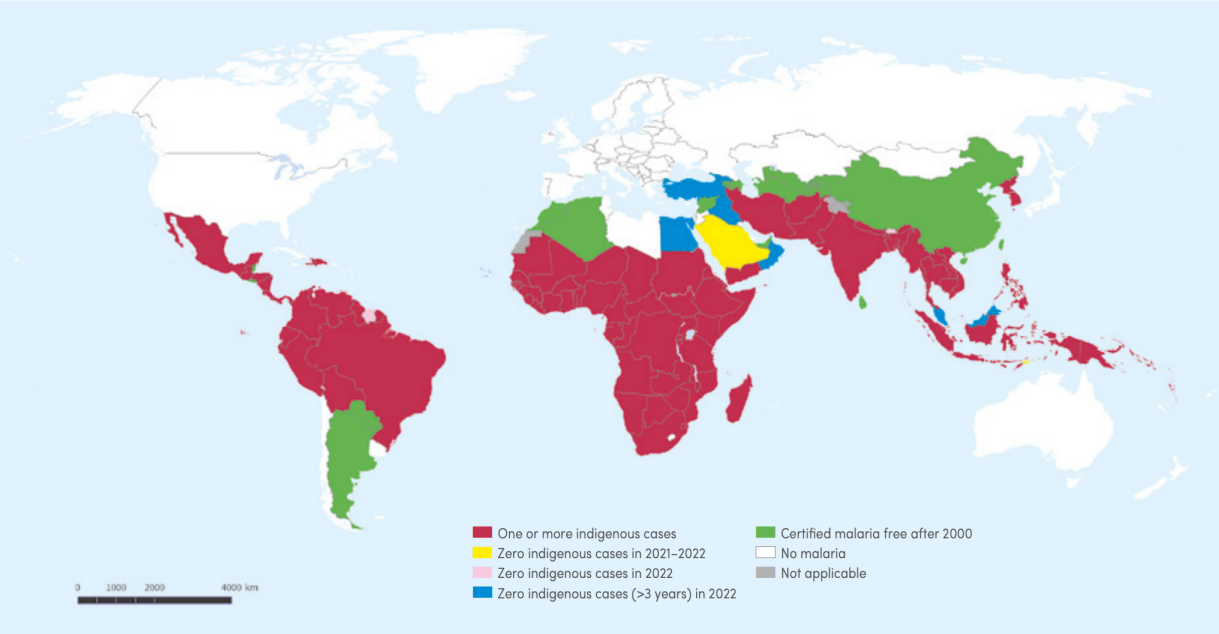

Figure 1. Malaria Worldwide Distribution with countries and areas with indigenous cases in 2000 and their status by 2022 according to WHO [5]. Countries and areas in red had one or more indigenous cases in 2022. Countries and areas in red had no reported indigenous cases in 2022. Countries and areas in yellow had zero indigenous cases from 2021 to 2022. Countries and areas in blue had no indigenous cases for the last three years from 2022 and are considered to have eliminated malaria in 2022. Countries and areas in green are considered malaria-free since 2000. Countries and areas in white have no indigenous malaria.

1.1.3 Malaria Pathogens

In 1880, French physician Charles Louis Alphonse Laveran discovered *Plasmodium* as the malaria pathogen after observing round pigmented bodies with flagella-like filaments moving in the blood of infected patients, earning him the Nobel Prize in Medicine in 1907 [1].

Plasmodium is a genus of over 200 protozoan parasite species that infect various vertebrates and are transmitted by mosquitoes through human-to-human (i.e., anthroponotic) and animal-to-human (i.e., zoonotic) routes [6]. Among them, five species, *P. falciparum*, *P. vivax*, *P. malariae*, *P. ovale* and *P. knowlesi,* cause malaria in humans [6]. *P. falciparum*, the most lethal, is prevalent in Africa and leads to severe complications and high mortality rates [1]. *P. vivax* has a broader geographic range due to its ability to develop in mosquito vectors that withstand colder climates and higher altitudes, making it dominant outside sub-Saharan Africa [1]. Additionally, *P. vivax* and *P. ovale* can remain dormant in the liver as hypnozoites, reactivating weeks or years later and causing malaria relapses [7]. *P. knowlesi*, though primarily found in macaque monkeys, can infect humans and is a significant concern in Southeast Asia [6].

1.1.4 Life Cycle of *Plasmodium spp.*

The *Plasmodium* life cycle involves a vertebrate host and an *Anopheles* mosquito vector, which transmits the parasite via blood meals (see Figure 2.) [6].

When an infected female *Anopheles* mosquito bites a host, *Plasmodium* sporozoites from the mosquito saliva enter the bloodstream and travel to the liver, where they infect hepatocytes [8]. Inside hepatocytes, sporozoites multiply asexually, forming schizonts that release thousands

of new progenies, known as merozoites [6]. In *P. vivax* and *P. ovale* infections, some sporozoites become dormant hypnozoites that reactivate later [9].

Once the infected hepatocytes rupture, merozoites enter the bloodstream and infect erythrocytes [8]. Within these cells, merozoites develop into ring-stage trophozoites and mature into schizonts, which burst to release more merozoites that continue to infect new erythrocytes, repeating the cycle [8]. Some trophozoites differentiate into male and female gametocytes, a process known as gametocytogenesis [6].

When a female *Anopheles* mosquito feeds on an infected host, it ingests these gametocytes, which mature into gametes in the mosquito's midgut [8]. The midgut lumen environment triggers the gametes to become fertile, with male microgametes flagellating to reach and fertilize female macrogametes, forming a zygote [9]. The zygote undergoes genetic recombination and transforms into a motile ookinete, which crosses the midgut wall and forms an oocyst on the outer surface [6]. The oocyst produces thousands of sporozoites via sporogony, which, once released, migrate to the mosquito’s salivary glands, ready for transmitting to a new host [6].

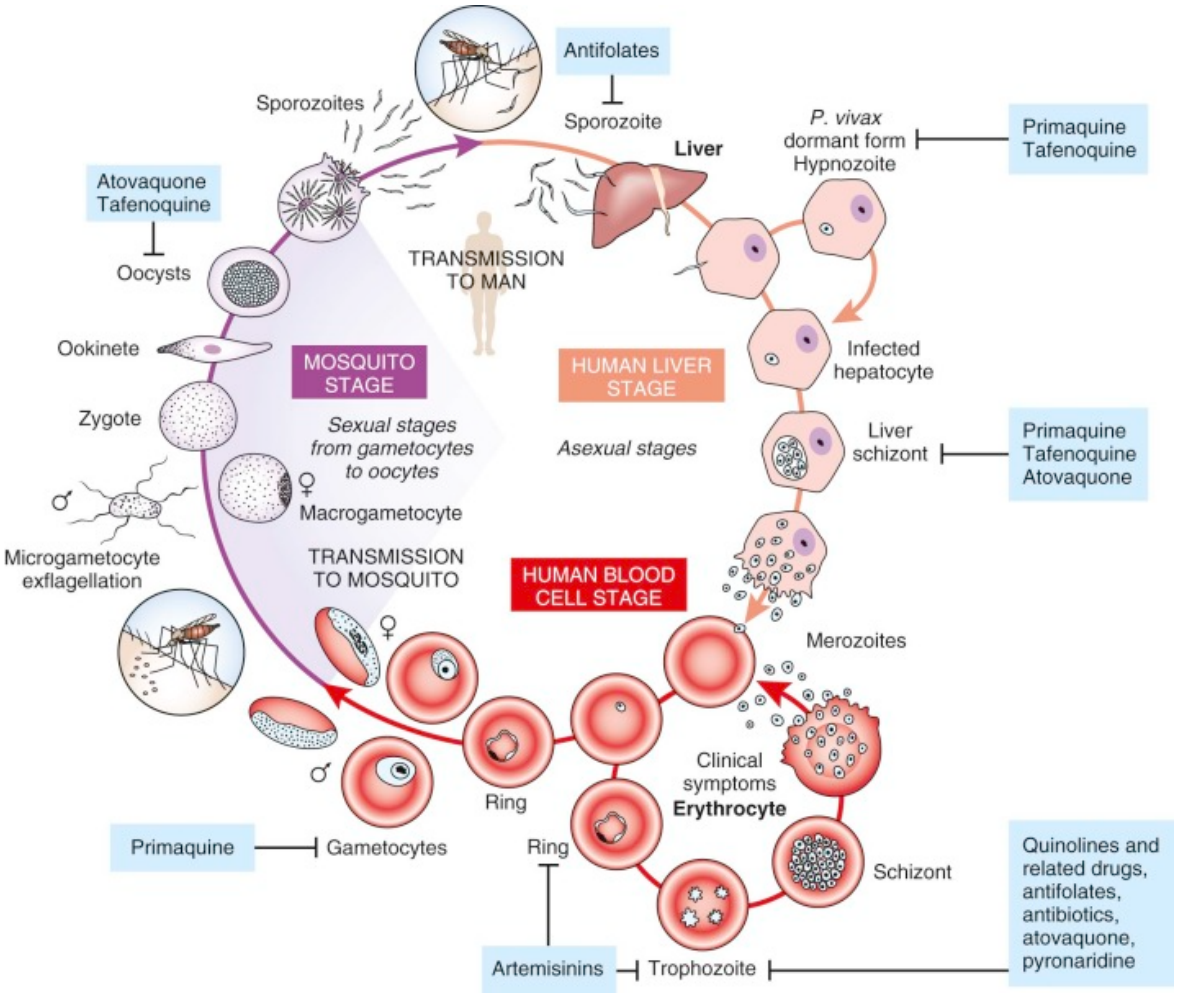

Figure 2. The Life Cycle of *Plasmodium falciparum* with antimalarial drugs specific to different parasitic stages [88]. This diagram illustrates the life cycle of *P. falciparum* with human being the specific vertebrate host. Transmission begins with the injection of sporozoites into humans during a mosquito bite. In the liver stage, sporozoites infect hepatocytes, where they develop into liver schizonts and release merozoites into the bloodstream.
During the blood stage, merozoites invade erythrocytes and progress through ring, trophozoite, and schizont stages, causing the clinical symptoms of malaria. Some parasites differentiate into gametocytes, which are ingested by mosquitoes during a blood meal, completing the transmission cycle. Key antimalarial drugs are indicated in blue boxes, targeting specific parasite stages such as sporozoites, hypnozoites, liver schizonts, erythrocytic stages (ring and trophozoite), gametocytes in humans, and oocysts in mosquitoes [88].

1.1.5 Malaria Symptoms

The *Plasmodium* life cycle in vertebrate hosts includes an initial asexual stage in the liver and a blood stage, with clinical symptoms appearing only during the latter [10]. During this blood stage, infected erythrocytes burst to release merozoites and toxic by-products like glycosylphosphatidylinositols (GPI) and hemozoin produced by the parasites [11]. Additionally, immune cells recognize other pathogen-associated molecular patterns (PAMPs) like parasitic nucleic acids and damage-associated molecular patterns (DAMPs) like endogenous heme, uric acid, host nucleic acids, and extracellular vesicles via their toll-like receptors or when phagocytosing infected erythrocytes [12]. This activation triggers the innate cells to release pro-inflammatory cytokines and chemokines [12]. While these immune responses aid in parasite clearance, they also lead to nonspecific symptoms seen in uncomplicated malaria, such as fatigue, headache, muscle aches, vomiting, diarrhea, chills, sweating, and recurrent fever [13].

If untreated, uncomplicated malaria can escalate to severe malaria, presenting with splenomegaly, anemia, thrombocytopenia, hypoglycemia, and pulmonary, liver, renal or neurological dysfunction, potentially leading to death [11, 14]. Disease severity depends on the host's immune status, parasitemia level, and infecting species, with *P. falciparum* being the deadliest, as it evades splenic clearance by sequestering infected erythrocytes in capillaries and venules [14, 15]. Parasitic proteins like histidine-rich protein (PfHRP) and erythrocyte membrane protein 1 (PfEMP1) enable this cytoadherence by binding to host endothelial receptors such as ICAM-1 and CD36, anchoring the infected cells to vessel walls [11]. Although chemokines recruit monocytes to clear these cells, PAMPs and DAMPs trigger excessive cytokine release, like TNF and IL-1β, which increase endothelial receptor expression and enhance cytoadherence, promoting further sequestration [12]. PfEMP1 also promotes rosetting,

where uninfected erythrocytes and thrombocytes cluster around infected cells, helping the parasite evade immune detection [16]. Together, sequestration and rosetting obstruct microvasculature, induce localized inflammation, increase vascular permeability, and deprive tissues of oxygen and nutrients, leading to organ dysfunction, which can be fatal, especially in cerebral malaria [15].

1.1.6 Diagnosis of Malaria

Diagnosing malaria solely through clinical symptoms is unreliable, as it often resembles other tropical diseases and can be complicated by coinfections of other pathogens [8]. Light microscopy remains the gold standard, enabling direct visualization of *Plasmodium* parasites in Giemsa-stained blood smears and detecting erythrocyte abnormalities with high sensitivity and cost-effectiveness [17]. WHO-recommended rapid diagnostic tests (RDTs) identify malaria antigens like HRP-2, LDH, and aldolase using dye-labeled antibodies [17]. While affordable and user-friendly, RDTs' accuracy varies due to factors like parasite density and operator handling, potentially causing false results [17]. Advanced methods like enzyme-linked immunosorbent assay (ELISA), flow cytometry, and polymerase chain reaction (PCR) offer greater precision but require specialized laboratory resources [17].

1.1.7 Treatments against Malaria

Currently, three main categories of antimalarial drugs are available: quinoline derivatives, antifolate compounds, and artemisinin derivatives [18].

Quinoline derivatives include quinine, lumefantrine, CQ, mefloquine, and others [18]. Most target the erythrocytic stage, except primaquine, which acts against the hepatic stage and gametocytes [8]. These compounds hinder hemozoin formation, a critical process for detoxifying heme, as they cap growing hemozoin crystals and bind to free heme, thereby blocking heme conversion and poisoning the parasite [8].

Antifolate drugs, divided into two classes, disrupt the production of tetrahydrofolate, a vital cofactor for synthesizing nucleic acids and amino [8]. Class I agents, like sulfanilamide and sulfadoxine, inhibit dihydropteroate synthase (DHPS), preventing it from making dihydrofolic acid, a precursor for tetrahydrofolate [8, 19]. Class II antifolates, such as proguanil and pyrimethamine, target dihydrofolate reductase (DHFR), blocking dihydrofolate conversion into tetrahydrofolate in both hepatic and erythrocytic parasites [8, 20]. While DHPS is *Plasmodium*-specific, human and parasitic DHFR enzymes are different enough to enable selective inhibition [19].

The prevailing theory for the mechanism of artemisinin derivatives suggests that they damage parasitic proteins and membranes through alkylation and lipid peroxidation with free radicals produced upon interacting with iron from heme [21]. Unlike other drugs, artemisinin targets multiple parasite processes, including hemoglobin digestion, glycolysis, nucleic acid synthesis, antioxidant defence, and components of the electron-transport chain [21]. This multi-target action makes them highly potent, reducing the parasite burden by 10,000-fold every 48-hour cycle in *P. falciparum* [22].

Artemisinin derivatives are rapidly cleared from the body, with a short half-life of about 45 minutes [23]. This quick elimination reduces the risk of developing drug-resistant parasites, as prolonged exposure to sub-inhibitory drug levels increases resistance [23]. To maintain their

effectiveness, the WHO recommends artemisinin-based combination therapies (ACTs), which combine artemisinins with longer-acting antimalarials that clear any remaining parasites [22]. This strategy also lowers the risk of resistance to partner drugs and improves treatment efficacy by targeting multiple pathways [24]. The WHO currently endorses six ACTs: artesunate combined with amodiaquine, sulfadoxine-pyrimethamine, mefloquine, or pyronaridine; artemether with lumefantrine; and dihydroartemisinin with piperaquine [24].

1.1.8 Malaria Prevention

Chemoprophylaxis with antimalarial agents help prevent malaria for non-immune travellers and endemic area residents [25]. For travellers, the CDC recommends atovaquone/proguanil, doxycycline, mefloquine, CQ, primaquine, and tafenoquine, with the first three being the most prescribed for CQ-resistant *P. falciparum* [25, 26]. Proper adherence before, during, and after travel is essential for effective prophylaxis, though side effects and compliance issues, such as forgetfulness, often pose challenges [25]. Severe side effects, such as mefloquine-induced psychosis or hemolytic anemia in individuals with glucose-6-phosphate dehydrogenase (G6PD) deficiency, complicate drug selection, which also depends on destination, health status, and cost [26-28]. Pregnant women are advised to avoid endemic regions, as prophylaxis does not ensure complete protection [27].

For endemic areas, chemoprophylaxis includes intermittent preventive treatment (IPT) for pregnant women and infants, seasonal malaria chemoprevention (SMC) for children, and mass drug administration (MDA) to entire communities [29]. Sulfadoxine-pyrimethamine is commonly used due to its affordability and long-lasting effects, while artemisinin-based

therapies support MDA efforts [30, 31]. However, drug toxicity, side effects, and rising resistance underscore the need for effective vaccines [8].

The WHO recommends the RTS-S/AS01 and R21/Matrix-M vaccines for children in high-transmission areas [32]. These vaccines combine fragments of the parasitic circumsporozoite protein, which coats the surface of sporozoites, with hepatitis B antigens to generate immune responses targeting *P. falciparum* before it infects red blood cells [8, 32].

Vector control remains a cornerstone of prevention. Insecticide-treated nets (ITNs) and indoor residual spraying (IRS) with long-lasting insecticides like pyrethroids, organophosphates, and carbamates effectively reduce transmission by killing mosquitoes [33]. Together, chemoprophylaxis, vaccination, and vector control provide comprehensive protection against malaria.

1.1.9 Antimalarials Resistance

A significant challenge in treating and preventing malaria is the emergence of antimalarial drug resistance in *Plasmodium* parasites [34]. Drug resistance enables parasites to survive or multiply even when exposed to recommended or higher drug doses despite the drugs being fully absorbed and acting effectively as intended on infected red blood cells [8].

The two most threatening malaria species, *P. falciparum* and *P. vivax,* tolerate many available antimalarial drugs [24]. *P. falciparum* has developed resistance to quinolines, antifolates, and artemisinin derivatives, while *P. vivax* is resistant to CQ, primaquine, and antifolates [24].

CQ, a quinoline derivative and successful synthetic alternative to quinine, served as the first-line malaria treatment before artemisinin-based therapies became available [35]. However, resistance to CQ emerged in the 1960s in South America and Southeast Asia and spread to Africa in the 1970s due to widespread use [34]. Mutations in the *PfCRT* (*Plasmodium falciparum* Chloroquine Resistance Transporter) protein on the digestive vacuole (DV) membrane enable *P. falciparum* to expel quinoline antimalarials more effectively, conferring resistance [34]. Another protein involved in resistance is *PfMDR1* (*Plasmodium falciparum* Multidrug Resistant Protein 1), an import transporter on the DV membrane [36]. Although its role is less understood, some researchers suggest that *PfMDR1* mutations reduce drug import, while others believe its overexpression traps cytosolic-targeting compounds inside the vacuole [36].

The spread of CQ resistance led to the implementation of sulphadoxine and pyrimethamine, cost-effective antifolates still used in chemoprophylaxis [19, 37]. These drugs inhibit DHPS and DHFR enzymes necessary for amino and nucleic acid synthesis [19]. Point mutations in these enzymes quickly confer resistance by reducing drug-binding affinity [19]. Although studying these mutations and analyzing the crystal structures of mutant enzyme-drug complexes aids in redesigning and developing new antimalarials, the process remains expensive and time-consuming due to clinical trial requirements [19].

A critical threat to malaria control is resistance to artemisinin, a vital component of ACTs. Resistance primarily arises from mutations in the *Pfkelch13* gene, which reduce hemoglobin uptake and, consequently, lower heme production, an essential molecule for activating artemisinin but also a nutrient for the parasites [38]. These mutations slow parasite growth and induce a quiescent state during drug exposure, activating stress response pathways like the

unfolded protein response (UPR) and DNA repair mechanisms in the parasite to mitigate artemisinin toxicity [39]. Once artemisinin clears from the bloodstream, the parasites resume growth [22].

Since artemisinin resistance was first reported in Cambodia in 2008, it has spread across the Greater Mekong sub-region and now shows mutations in Africa [22]. This resistance increases the burden on partner drugs, which face higher parasite loads and a greater risk of developing or worsening resistance, potentially leading to treatment failure [22].

1.2 Oxidative Stress and Malaria

As *Plasmodium* species, notably *P. falciparum*, have developed mechanisms to resist antimalarial drugs, humans in malaria-endemic regions have also evolved genetic adaptations that offer some protection against malaria, albeit with certain drawbacks [40]. These adaptations include inherited hemoglobin abnormalities, such as sickle cell trait and thalassemias, and G6PD deficiency [41]. These conditions disrupt the redox balance in erythrocytes, impairing their ability to manage oxidative stress effectively [41].

Oxidative stress occurs when ROS overwhelm the body's antioxidant defences [42]. The unpaired electrons in ROS make them highly unstable, leading to indiscriminate damage to both host and parasitic cellular components [43].

Erythrocytes, which transport oxygen and mediate carbon dioxide, constantly encounter ROS [44]. Endogenously, ROS arise primarily from hemoglobin autoxidation, which releases superoxide anions ($O_2^{\bullet -}$), as well as from enzymatic activities of nicotinamide adenine

dinucleotide phosphate (NADPH) oxidase and xanthine oxidase [45]. Extracellular ROS derive from Fenton reactions between hydrogen peroxide and free heme iron, which is tightly regulated by proteins to maintain a low concentration [45].

In malaria-infected erythrocytes, parasites degrade hemoglobin to extract amino acids, releasing excess free heme and significantly increasing ROS production [43]. Additionally, xanthine oxidase activity intensifies during malaria infection, producing superoxide ($O_2 \cdot^-$) and hydrogen peroxide (H_2O_2), further amplifying oxidative stress [43]. These ROS trigger lipid peroxidation in both infected and uninfected erythrocyte membranes, rendering them rigid and less deformable, an essential property for erythrocytes to pass through narrow capillaries [43, 46]. The resulting rigidity marks erythrocytes for splenic clearance, contributing to anemia [11, 43]. However, ROS also serve as a defence mechanism, exploited by immune cells and artemisinin derivatives to kill parasites [43].

In hemoglobin abnormalities, genetic mutations either alter the amino acid sequence of the globin chain, such as in sickle cell trait (HbS), HbC, and HbE or disrupt the balance between α and β chain production, as seen in thalassemias [41]. The severity depends on how many of the four α-chain or two β-chain genes are affected [47]. For instance, heterozygous carriers of HbAS (sickle cell trait) benefit from protection against severe malaria without significant hematological issues, whereas homozygous carriers (HbSS) develop sickle cell disease (SCD) with severe anemia and painful crises [48].

Although the exact mechanisms remain unclear, hemoglobin abnormalities confer protection by increasing oxidative stress in infected erythrocytes [48]. This redox imbalance reduces adhesins and PfEMP1 on the erythrocyte surface and disrupts actin remodelling,

impairing protein export [48, 49]. These changes reduce cytoadherence, enhancing splenic clearance of infected erythrocytes [49].

Similarly, deficiency in G6PD, a housekeeping enzyme that catalyzes the production of NADPH, a vital cofactor for regenerating reduced GSH, a critical antioxidant that helps erythrocytes to survive oxidative stress, also leads to redox imbalance, thereby conferring protection against malaria [50].

In conclusion, while ROS serve as a defence mechanism exploited by the immune system and artemisinin derivatives to kill parasites, excessive ROS can damage host cells, contributing to clinical symptoms [43].

1.3 Antioxidant Systems in Erythrocytes

Erythrocytes combat these ROS using a network of antioxidant systems (see Figure 3.) [45]. Superoxide dismutases (SODs) convert superoxide anions ($O_2^{\bullet -}$) into hydrogen peroxide (H_2O_2), which is detoxified into water by catalase (Cat), glutathione peroxidase (GPx), and peroxidase (Prx) [45]. GPx uses GSH as a cofactor to reduce H_2O_2 and lipid hydroperoxides, forming oxidized glutathione (GSSG), which glutathione reductase (GR) regenerates back to GSH using NADPH from the pentose phosphate pathway (PPP) [45]. Similarly, Prx detoxifies H_2O_2 and other peroxides, with its oxidized form reduced by thioredoxin (Trx), which thioredoxin reductase (TR) regenerates using NADPH [45]. Glutaredoxin (Grx) also uses GSH to prevent irreversible protein damage through glutathionylation, forming a reversible mixed disulfide (Protein-S-SG) that it can reduce back with GSH to restore protein activity [45].

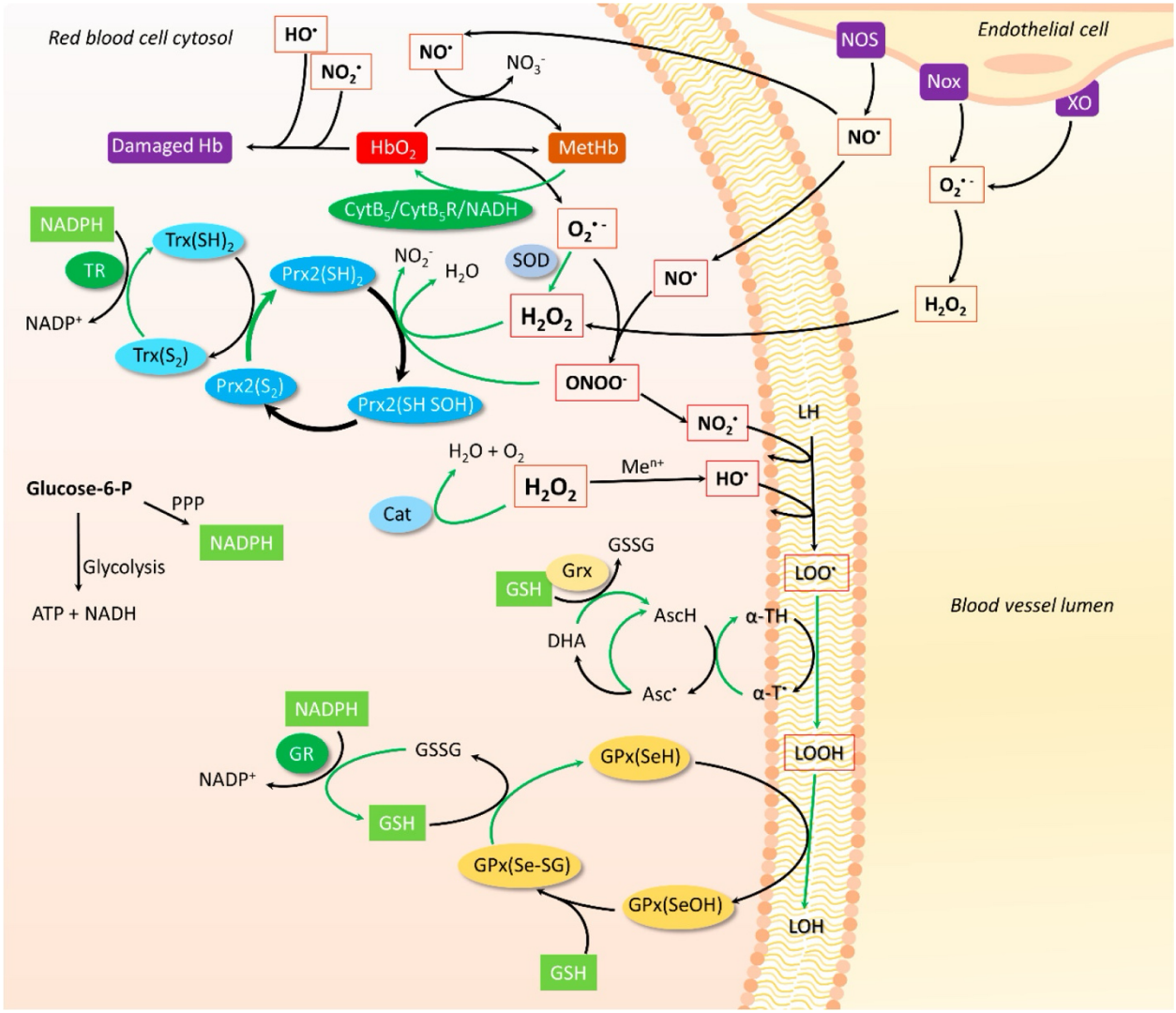

Figure 3. Antioxidant systems and redox regulation pathways in erythrocytes with ROS shown in red boxes, enzymatic antioxidants shown in ovals of different colors, reduction reactions shown by green arrows [45]. This figure highlights the intricate network of redox reactions and antioxidant systems that maintain cellular redox balance. In erythrocytes, the PPP uses glucose-6-phosphate (G6P) to generate NADPH, which fuels GR for GSH regeneration. GSH neutralizes ROS and lipid hydroperoxides (LOOH), with GPx reducing these oxidants to non-toxic forms. Trx, TR, and Prx also mitigate oxidative stress by scavenging hydrogen peroxide (H_2O_2) and repairing oxidized proteins. Methemoglobin (MetHb) is detoxified via MetHb reductase pathways. In endothelial cells, enzymes like nitric oxide synthase (NOS) and xanthine oxidase (XO) generate reactive nitrogen species (RNS) and ROS, contributing to vascular oxidative stress. SOD catalyzes the dismutation of superoxide (O_2^-) to H_2O_2, which is further detoxified by Cat and GPx. Interactions between erythrocytes and endothelial cells ensure a dynamic exchange of ROS/RNS, emphasizing the protective role of erythrocyte antioxidant systems against vascular oxidative damage.

1.4 Modulation of Glutathione via Transporters

GSH synthesis requires two ATP-dependent steps: the rate-limiting step where glutamate cysteine ligase (GCL) forms γ-glutamylcysteine, followed by glutathione synthetase combining it with glycine to produce GSH [45]. Transporters regulate GSH levels by importing amino acid precursors (cysteine, glycine, glutamate) essential for its synthesis and exporting GSH/GSSG [45]. Targeting these transporters can lower GSH levels, mimicking the oxidative stress seen in G6PD deficiency, which protects against malaria.

1.4.1 Cystine/Glutamate Antiporter System Xc-

Cysteine, a vital constituent of GSH, circulates in the blood as oxidized di-peptide cystine and relies on the cystine/glutamate antiporter system xc− (Sxc−) for cellular import (see Figure 4.) [51]. Sxc- or system xCT, is a sodium-independent cystine/glutamate antiporter that takes in one cystine in exchange for one glutamate out (see Figure 4.) [51]. This cystine is then reduced to cysteine by GSH or thioredoxin reductase 1 for GSH synthesis [52].

System xCT belongs to the family of heteromeric amino acid transporters (HAT) that consist of a heavy subunit (SLC3) and a light subunit (SLC7) connected by an extracellular disulfide bond [53]. The heavy subunit, known as 4F2hc, CD98 or SLC3A2, facilitates the trafficking of the antiporter to the plasma membrane and stabilizes the light subunit [53]. Structurally, it consists of a single transmembrane helix with a glycosylated extracellular C-terminus and an intracellular N-terminus [53]. The light chain, SLC7A11 or xCT, is a polytopic membrane protein that defines the transporter's substrate specificity [53]. It features 12 transmembrane domains with intracellular C- and N-termini [53]. These domains change the

transporter's shape, enabling it to access ligands between intracellular and extracellular environments [53].

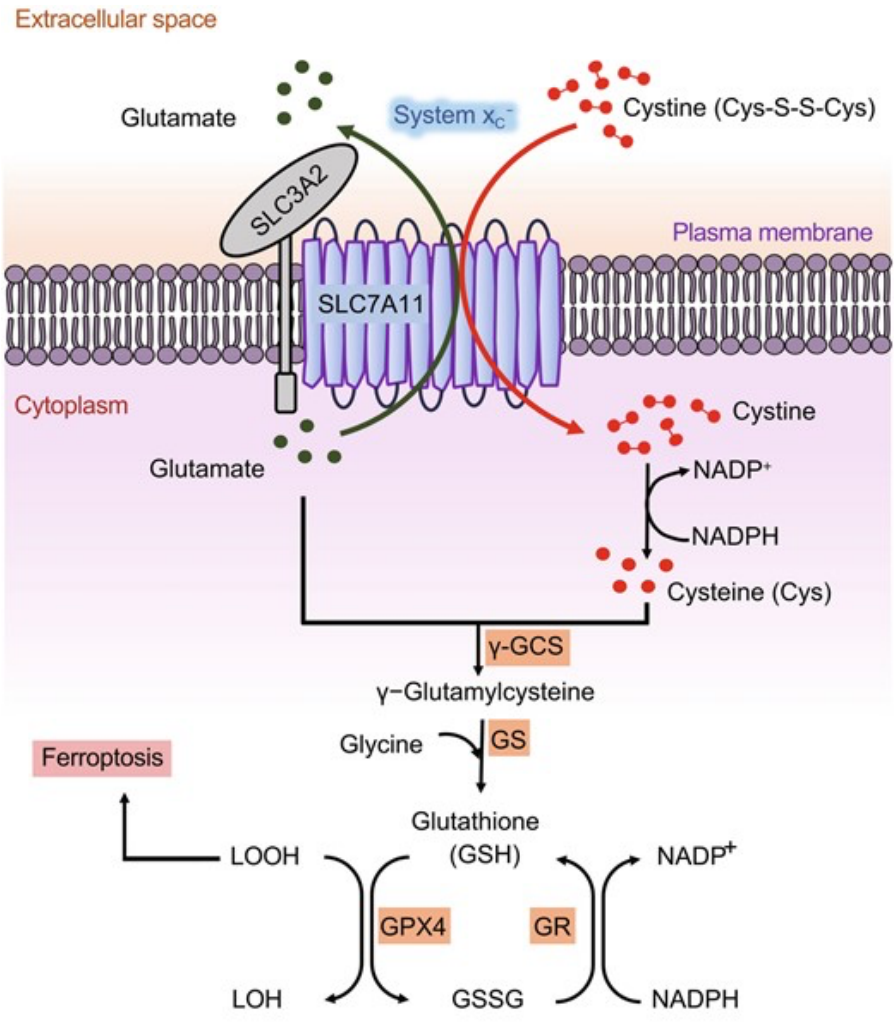

Figure 4. Structure and Function of System xc⁻ [89]. This diagram illustrates the role of the SLC7A11 subunit of System xc⁻ in importing extracellular cystine in exchange for intracellular glutamate. Once inside the cell, cystine is reduced to cysteine in a NADPH-dependent reaction. Cysteine, along with glutamate and glycine, serves as a precursor GSH synthesis via the γ-GCS and glutathione synthetase enzymes. GSH plays a pivotal role in detoxifying ROS and LOOH through glutathione peroxidase (GPX4), converting them into non-toxic forms like water and lipid alcohols (LOH). GR regenerates GSH from GSSG using NADPH as a reducing agent. Dysregulation in this pathway can lead to ferroptosis, a form of cell death driven by excessive lipid peroxidation.

Several inhibitors target system xCT, including carboxyphenylglycine (CPG) analogs, erastin, sorafenib, and sulfasalazine (SSZ) [54]. Notably, SSZ, widely used to treat ulcerative colitis, Crohn's disease, and rheumatoid arthritis, and the anticancer drug sorafenib are both FDA-approved [55]. However, sorafenib causes significant adverse effects [55]. SSZ, a pro-drug, is metabolized *in vivo* into 5-aminosalicylic acid and sulfapyridine, which exhibit anti-inflammatory properties and inhibit Sxc^-, likely by acting as a competitive substrate [56].

1.4.2 ATP-binding Cassette (ABC) Subfamily C1 Transporter

In addition to reducing the availability of cystine for GSH synthesis, increasing GSH efflux through multidrug resistance-associated proteins (MRPs) further lowers intracellular GSH levels in erythrocytes [45]. MRPs, encoded by the ABCC genes, belong to the C subfamily of the ATP-Binding Cassette (ABC) transporter superfamily, which comprises seven subfamilies ranging from ABCA to ABCG [57]. These transmembrane transporters use adenosine triphosphate (ATP) as an energy source to transport substrates against their concentration gradients across cellular membranes [57].

Structurally, ABC transporters typically consist of two transmembrane domains (TMDs) and two intracellular nucleotide-binding domains (NBDs) (See Figure 5.) [57]. Each TMD contains six membrane-spanning α-helices connected by intra- and extracellular loops, while substrate binding induces conformational changes in the TMDs to facilitate transport across the membrane [57]. The NBDs hydrolyze ATP to provide the energy required for these conformational shifts and contain a Walker-A motif (P-loop) for ATP phosphate binding, along with a conserved LSGGQ sequence unique to ABC transporters [57].

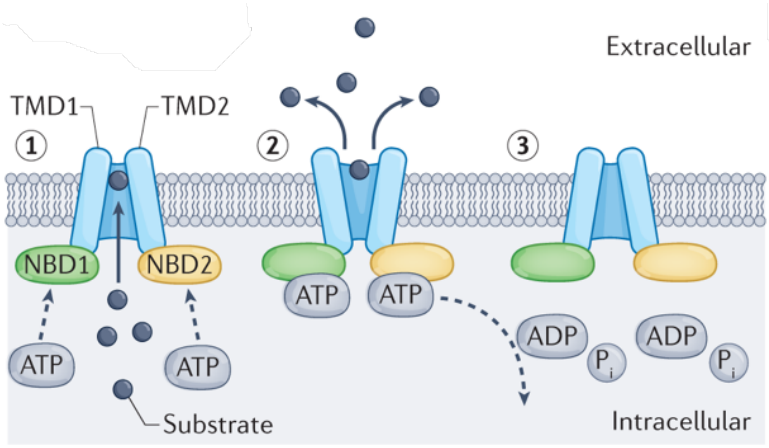

Figure 5. Structure and Function of ABCC1 [90]. This figure illustrates the stepwise mechanism of substrate transport by ABC transporters. (1) The transporter, consisting of two TMDs (TMD1 and TMD2) and two NBDs (NBD1 and NBD2), binds a substrate at its intracellular binding site. ATP molecules bind to the NBDs, initiating a conformational change. (2) This change enables the transporter to transition into an outward-facing conformation, allowing the substrate to be released into the extracellular space. (3) Hydrolysis of ATP to ADP and inorganic phosphate (P_i) restores the transporter to its original inward-facing conformation, resetting the cycle for subsequent substrate transport.

Within the ABCC subfamily, erythrocytes express ABCC1 (MRP1) and ABCC4 (MRP4), with mass spectrometry also identifying ABCC5 (MRP5) and ABCC10 (MRP7) in the red blood cell membrane [45, 58]. These transporters play a critical role in maintaining cellular homeostasis by exporting various substrates and detoxifying harmful metabolites [57]. For instance, MRP4 mediates the efflux of endogenous signalling molecules like prostaglandins, leukotrienes, cyclic nucleotides, and folic acid [59]. Meanwhile, MRP1 regulates redox balance by exporting GSH, GSSG, and glutathione-conjugated organic anions [60]. However, these transporters also contribute to drug resistance, particularly in cancer, where their expression is often upregulated to excrete therapeutic xenobiotics [57].

Enhancing MRP1's ability to efflux GSH offers a promising strategy to replicate the protective effects against malaria observed in G6PD deficiency. Compounds such as

pharmacological drugs, antineoplastic agents, and flavonoids have been shown to accelerate MRP1-mediated GSH export from cells [61]. Among these, flavonoids, a diverse class of naturally occurring polyphenolic compounds derived from plants, demonstrate notable efficacy in promoting GSH binding to MRP1 and enhancing its efflux at lower concentrations (20–50 μM) compared to the pharmacological drug verapamil (100 μM) [61]. Additionally, flavonoids exhibit a better safety profile, avoiding the toxic side effects of verapamil, such as heart block, hypertension, and arrhythmia [61].

In a related study, apigenin (API), a flavonoid, was shown to induce MRP1-mediated GSH efflux in erythrocytes, leading to increased oxidative stress that inhibited the proliferation of both CQ-sensitive and CQ-resistant *P. falciparum* [62]. Furthermore, co-treatment with API and artemisinin significantly reduced the IC50 (half-maximal inhibitory concentration) of artemisinin required to inhibit *P. falciparum* proliferation, highlighting a potential synergistic effect between the two compounds [62].

2 Rationale and Objectives

Rationale

Malaria remains a significant global health challenge, caused by *Plasmodium* parasites and predominantly affecting low-income countries, where it remains a leading cause of death [5]. Current control strategies rely heavily on antimalarial drugs targeting parasitic metabolism. However, these approaches create evolutionary pressure on parasites, fostering drug resistance [63]. An alternative strategy involves targeting host factors, particularly mature red blood cells

(RBCs), which are less prone to mutations due to their dependence on tightly regulated erythropoiesis [64].

Parasites depend on host erythrocytes for survival, intensifying oxidative stress through their metabolism, which generates additional ROS [43]. Depleting antioxidants like GSH disrupts RBC defence mechanisms, triggering eryptosis and facilitating parasite clearance, as observed in G6PD deficiency [50, 65]. Enhancing GSH efflux using API, which activates ABCC1, has proven effective in reducing parasitic proliferation [62]. Additionally, inhibiting GSH synthesis with SSZ, which blocks system xc- to limit cysteine availability [56], may similarly impair *P. falciparum* proliferation.

Objectives

To test this hypothesis, we aimed to identify the effective concentrations of API and SSZ, both individually and in combination, that increase ROS levels in uninfected erythrocytes without inducing significant hemolysis. Furthermore, we sought to demonstrate that these concentrations inhibit the in vitro proliferation of CQ-sensitive and CQ-resistant *P. falciparum.* This study hypothesizes that API and SSZ increase ROS, selectively eliminating parasite-infected erythrocytes while sparing uninfected ones due to their high GSH levels [45].

3 Materials and Methods

Apigenin (≥95.0%, HPLC), sulfasalazine (97.0-101.5%), 2′,7′-Dichlorodihydrofluorescein diacetate, and hydrogen peroxide solution (30 wt. % in H2O, ACS reagent) were purchased from

Sigma- Aldrich. SYBR™ Green I nucleic acid gel stain (10,000X concentrate) was purchased from Invitrogen™. Human A+ RBCs were obtained from Interstate Blood Bank Inc. (Memphis, TN, USA) and Blood4Research facility (Vancouver, BC, Canada).

3.1 ROS Detection in Erythrocytes

The oxidation-sensitive fluorescent dye 2′,7′-Dichlorodihydrofluorescein diacetate (DCFH2-DA) was used to assess the effect of API and/or SSZ on intracellular ROS levels in uninfected erythrocytes. This cell-permeable, non-fluorescent probe can be hydrolyzed by intracellular esterases to form DCFH, a non-fluorescent intermediate [66]. DCFH can then be converted into highly fluorescent DCF upon oxidation by ROS, enabling the detection and quantification of ROS within cells [66].

Erythrocytes were washed twice with RPMI 1640 Medium without phenol red (Gibco™) and aliquoted to a concentration of 1×10^7 cells/mL per reaction for ROS detection. API and SSZ were initially dissolved in 100% DMSO (Thermo Scientific Chemicals) and subsequently diluted to the desired concentrations in a 1:1 mixture of DMSO and RPMI-1640 medium without phenol red. Erythrocytes were incubated for 23.5 hours at 37°C in the presence or absence of API and/or SSZ, with DMSO as the negative control, and 100 µM H_2O_2 as the positive control. A 5 mM stock solution of H_2DCFDA was freshly prepared in 100% DMSO and diluted to the desired concentration with PBS. Both untreated and treated erythrocytes were incubated with 50 µL of H_2DCFDA at a final concentration of 10 µM for 30 minutes, followed by two washes with 1× ice-cold PBS. After washing, erythrocytes were centrifuged at 2000 rpm for 5 minutes, resuspended in 100 µL ice-cold PBS, and transferred to a black 96-well plate with a transparent

flat bottom. The plate was read using a SYNERGY H4 hybrid microplate reader (BIOTEK) at 504 nm excitation and 530 nm emission after 1 minute of slow orbital shaking.

3.2 Hemolytic Assay

Since API and SSZ are yellow and orange when dissolved, respectively, assessing their hemolytic activity using the conventional Harobe method, which measures released hemoglobin at 405 nm, resulted in significant background interference due to the compounds' inherent colours. To overcome this, quantitative hemolysis assays were performed by measuring optical density (OD) at 650 nm, which detects erythrocytes' density, using an Infinite® 200 PRO (Tecan) microplate reader. Higher OD650 values indicate lower levels of hemolysis (i.e., more intact erythrocytes present), while lower OD650 values suggest increased hemolysis (i.e., fewer intact erythrocytes) [67].

API and/or SSZ, initially prepared in 100% DMSO, were first diluted to 2X the highest desired concentration in a 1:1 mixture of DMSO and RPMI 1640 medium without phenol red. The compounds were then further diluted to the desired concentrations in a transparent 96-well plate using a twofold serial dilution method, with a final volume of 100 µL per well. A 4% hematocrit erythrocyte solution was prepared in RPMI 1640 medium without phenol red, and 100 µL of this solution was added to each well, resulting in a final hematocrit of 2% and a total volume of 200 µL (100 µL of test compound and 100 µL of erythrocyte solution). To determine the relative percentage of hemolysis, 1% Triton X-100 was used as the positive control. The plate was incubated at 37°C for 24 hours and then read for absorbance at 650 nm after 30 seconds of orbital shaking.

3.3 *P. falciparum* Cultivation

CQ-sensitive (3D7) and CQ-resistant (Dd2) strains of *P. falciparum* were maintained in continuous culture using the modified protocol of Trager and Jensen [68]. Parasites were cultured in human A+ RBCs at 4% hematocrit in complete parasite medium (CPM), comprising RPMI 1640 medium (Gibco™) with 2 mM L-glutamine, 25 mM HEPES, 0.5% (w/v) AlbuMax I, and 0.1 mM hypoxanthine. Cultures were incubated at 37°C under a humidified, reduced-oxygen atmosphere (92% N_2, 5% CO_2, and 3% O_2). CPM was replaced daily or every 2–3 days, depending on parasitemia levels, as determined by examining blood smears stained with a Diff-Quick stain kit (Marketlab™) under light microscopy. Parasitemia was maintained below 10%, with ≤ 5% used for routine culture and 5–10% used for d-sorbitol synchronization and freezing.

3.4 D-sorbitol synchronization of *P. falciparum*

D-sorbitol selectively lyses trophozoite- and schizont-stage parasites via osmotic stress, enabling synchronization of cultures to ≥ 70% ring-stage *P. falciparum* parasites [69]. Briefly, asynchronous cultures with ≥ 5% parasitemia, predominantly containing ring-stage parasites (6–10 hours post-invasion), were centrifuged to remove CPM and resuspended in 5% d-sorbitol for 10 minutes at 37°C. Following treatment, cultures were washed twice with incomplete parasite medium (RPMI 1640 medium with 2 mM L-glutamine and 25 mM HEPES), resuspended in CPM, and maintained as described above.

3.5 SYBR Green I®-based Parasite Growth Inhibition Assay

Since uninfected erythrocytes lack a nucleus and mitochondria, and therefore contain no DNA, the SYBR Green I® assay, which binds specifically to double-stranded DNA, offers a simple and effective method to quantify parasite proliferation, as only parasitic DNA is detected [70]. Higher parasitemia corresponds to increased DNA content, resulting in a stronger fluorescence signal [70].

To evaluate the effects of drugs on parasite proliferation *in vitro*, SYBR Green I® assays were performed following the protocol by Carmony L. et al. [71], with some modifications. A 10 mM stock solution of CQ, used as the positive control, was prepared in sterile Milli-Q water, while 100 mM and 250 mM stock solutions of API and SSZ, respectively, were prepared in 100% DMSO. 4X Working solutions of these compounds were diluted from their respective stock solutions with CPM, resulting in starting concentrations of 400 nM for 3D7 and 8 µM for Dd2 strains for CQ, 800 µM for API, and 3200 µM for SSZ. An aliquot of 100 µL CPM was added to each well in a black 96-well microtiter plate, with the first row designated as the negative control containing uninfected erythrocytes and the second row as the positive control containing infected erythrocytes. Compounds (CQ, API, or SSZ) were serially diluted twofold into test wells in triplicate by transferring 100 µL of each drug solution. Subsequently, 100 µL of synchronized ring-stage cultures at 4% hematocrit and 0.5% parasitemia were added to the positive control and test wells, resulting in a final hematocrit and parasitemia of 2% and 0.25%, respectively. 100 µL of uninfected erythrocytes at 4% hematocrit were added to the negative control wells. The plate was incubated at 37°C under 92% N_2, 5% CO_2, and 3% O_2 for 72 hours. After incubation, the plates were sealed with aluminum foil and frozen at -80°C for 15 minutes to halt parasite activity. Once thawed, 50 µL of 5X lysis buffer (20 mM Tris, pH 7.5, 5 mM

EDTA, pH 8.0, 1.6% Triton X-100, 0.16% saponin) containing SYBR (0.5 µL of 10,000× SYBR® Green I per 1 mL of lysis buffer) was added to each well to lyse and stain the parasites. The plate was incubated in the dark at room temperature for 1 hour and read from the top for fluorescence signals using a SYNERGY H4 hybrid microplate reader (BIOTEK) with an excitation wavelength of 497 nm and an emission wavelength of 520 nm after 30 seconds of slow orbital shaking. Data analysis was conducted using Prism 13.0 (GraphPad Software) to calculate the half-maximal inhibitory concentration (IC50) of each drug/compound required to inhibit parasite growth by 50%. All graphs represent the mean ± SD of three independent experiments performed in triplicate.

3.6 Statistical Analysis

Statistical analyses were performed by one-way or two-way analysis of variance (ANOVA) using GraphPad Prism v.10.2.2.

4 RESULTS

4.1 Effects of DMSO on Uninfected Erythrocytes

To assess whether DMSO, the solvent used, generates ROS or causes hemolysis, erythrocytes were incubated with increasing concentrations of DMSO for three hours. ROS levels were measured using H_2DCFDA fluorescence as outlined in the ROS detection assay, and cell density was evaluated as described in the hemolytic assay.

Figure 6 illustrates the percentage differences in fluorescence between erythrocytes treated with varying concentrations of DMSO and the H_2DCFDA negative control, which contains 0.2% DMSO. A negative difference indicates that the treatment reduced ROS levels in erythrocytes, resulting in lower fluorescence, whereas a positive difference reflects an increase in ROS levels and higher fluorescence. Although treatment with 1.125% DMSO increased ROS levels by 13.92% compared to the dye control, statistical analysis using one-way ANOVA revealed that this difference was insignificant. These results suggest a negative correlation between % DMSO treatment and ROS levels, with significant reductions observed at concentrations above 2.25% DMSO. Specifically, 2.25% DMSO reduced ROS by 22.27% ($p < 0.001$), while 4.5% and 9% DMSO reduced ROS by 72.66% and 96%, respectively ($p < 0.0001$).

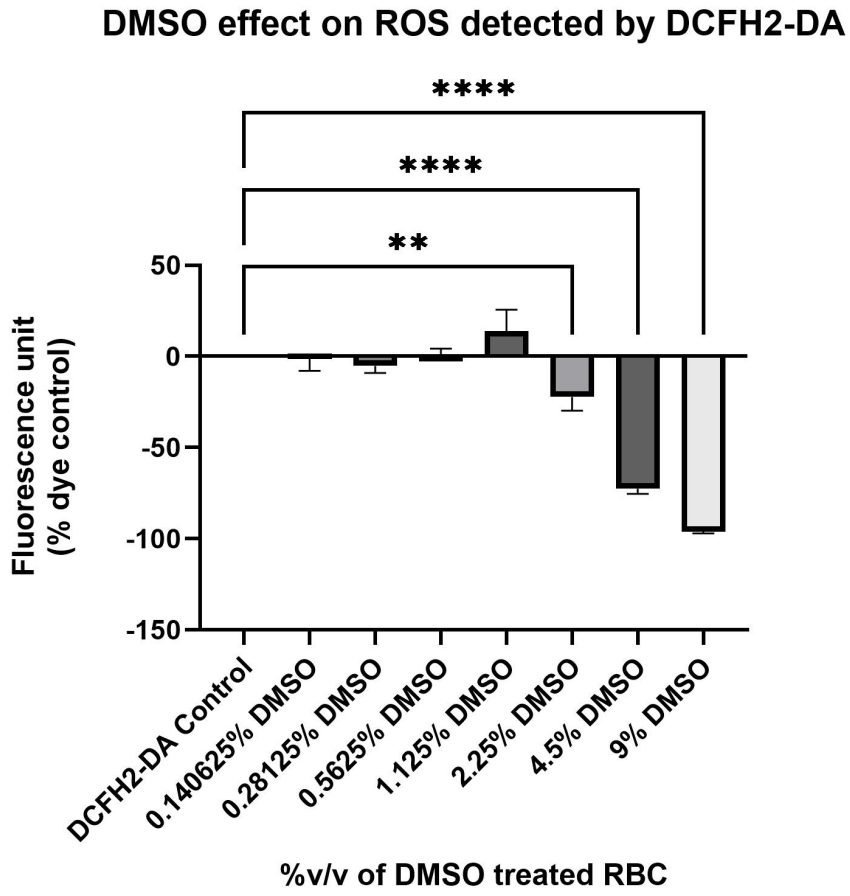

Figure 6. The effect of DMSO on intracellular ROS levels in uninfected erythrocytes. Erythrocytes were incubated in RPMI 1640 medium without phenol red for three hours at 37°C with increasing concentrations (% v/v) of DMSO. Intracellular ROS levels were measured using 10 µM of the fluorescent probe H_2DCFDA, dissolved in DMSO and added at a final concentration of 0.2% v/v DMSO, serving as the negative control (baseline). Results are presented as the mean fluorescence values relative to the H_2DCFDA control. Error bars represent ± S.D. of one independent experiment performed in triplicate. Statistically significant differences compared to the control are denoted by **($p < 0.001$) and ****($p < 0.0001$).

Figure 7 shows the percentage differences in absorbance at 650 nm between erythrocytes treated with varying concentrations of DMSO and the H_2DCFDA negative control. A negative difference indicates that the treatment caused hemolysis, reducing the number of intact erythrocytes and lowering optical density (OD). Similar to ROS levels, the results in Figure 7 suggest a negative correlation between % DMSO treatment and cell density, with significant reductions observed at higher concentrations: 4.5% and 9% DMSO reduced cell density by 30.38% and 90.5%, respectively ($p < 0.0001$).

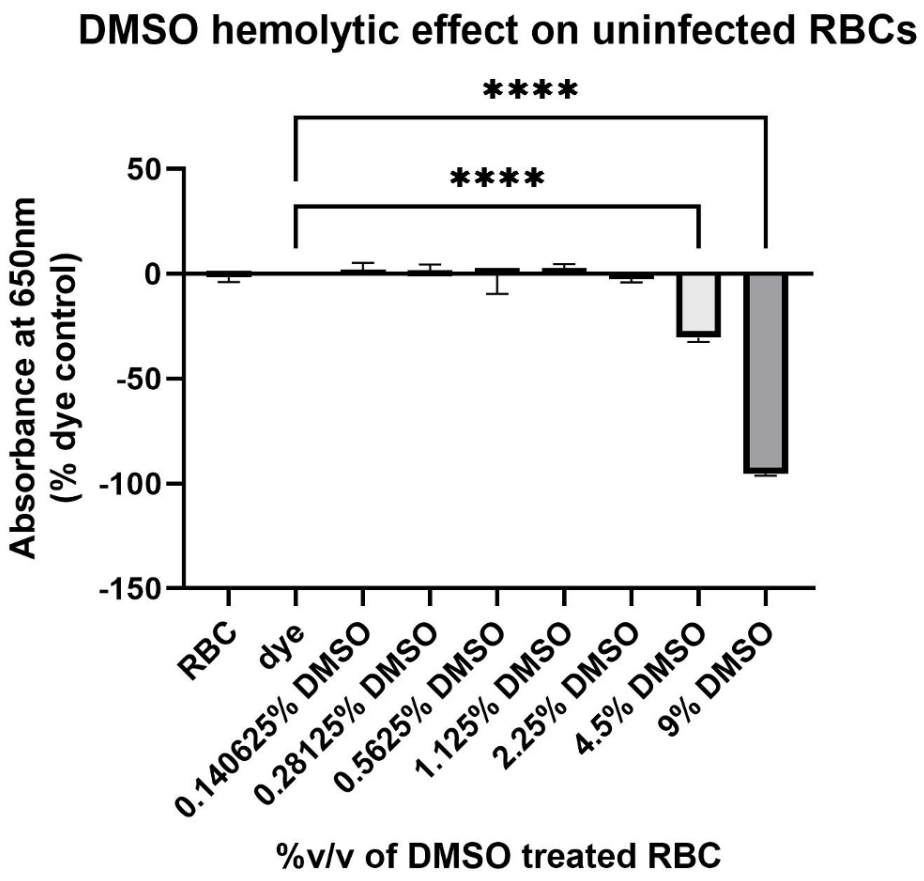

Figure 7. Hemolytic effect of DMSO on uninfected erythrocytes. Erythrocytes were incubated in RPMI 1640 medium without phenol red for three hours at 37°C with increasing concentrations (% v/v) of DMSO. Hemolytic activity was evaluated by comparing cell density, measured as absorbance at 650 nm, across DMSO-treated groups relative to the 10 µM H_2DCFDA dye control containing 0.2% v/v DMSO. Results are expressed as mean absorbance values relative to the H_2DCFDA control. Error bars represent ± S.D. from one independent experiment performed in triplicate. Statistically significant differences compared to the control are denoted by ****($p < 0.0001$).

4.2 Effects of Apigenin on Uninfected Erythrocytes

Having established that DMSO does not affect ROS levels or induce hemolysis at concentrations below 1% v/v, all API and SSZ preparations were formulated within this limit.

The effects of API on ROS levels and hemolysis were then assessed in erythrocytes incubated with increasing concentrations of API for 24 hours, following the previously described protocols.

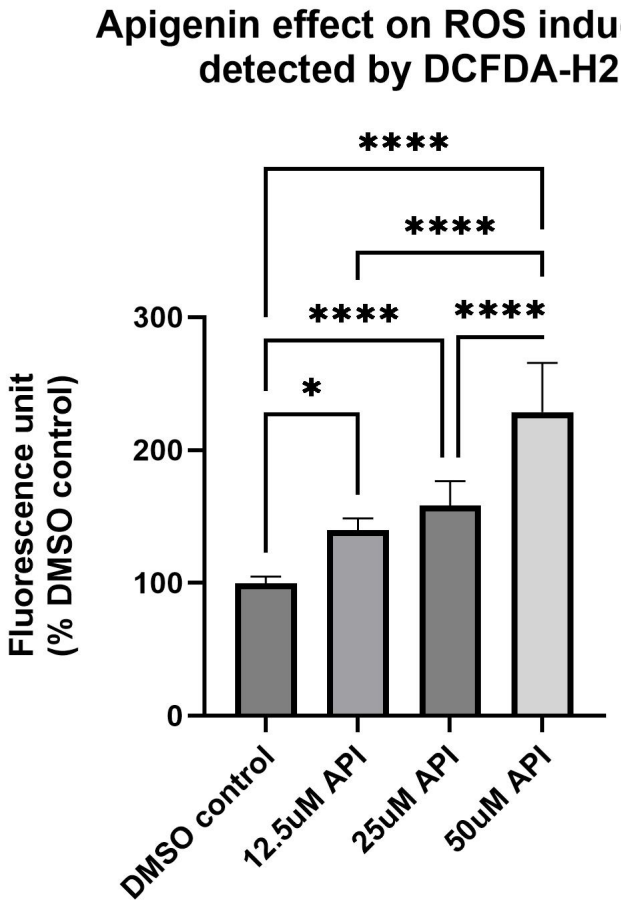

Figure 8. The effect of apigenin (API) on intracellular ROS levels in uninfected erythrocytes. Erythrocytes were incubated in RPMI 1640 medium without phenol red for 24 hours at 37°C with increasing concentrations (μM) of API. Intracellular ROS levels were measured using 10 μM of the fluorescent probe H_2DCFDA. Results are presented as the mean fluorescence values relative to the DMSO control. Error bars represent ± S.D. of two independent experiments performed in triplicate. Statistically significant differences are denoted by *($p < 0.01$) and ****($p < 0.0001$).

Figure 8 demonstrates that API induces a dose-dependent increase in intracellular ROS levels in uninfected erythrocytes. Using the DMSO control, containing 0.15% v/v DMSO, as the baseline, treatment with 12.5 μM, 25 μM, and 50 μM API led to progressively higher fluorescence intensities, reflecting elevated ROS levels. At 12.5 μM API, ROS levels increased

by 40%, showing a modest but statistically significant rise compared to the DMSO control ($p < 0.01$). Substantial increases of 58% and 129% were observed at 25 μM and 50 μM API, respectively, with ****($p < 0.0001$) compared to the control and lower API concentrations. However, the difference between 12.5 μM and 25 μM API was not statistically significant. In contrast, when compared to 50 μM API, ROS levels differed by 89% and 71% for 12.5 μM and 25 μM, respectively, with ****($p < 0.0001$).

Figure 9 illustrates the hemolytic effects of API on uninfected erythrocytes. The RBC control (no treatment) represents the baseline, indicating intact erythrocytes with 100% absorbance at 650 nm. In contrast, the positive control (1% Triton X-100) causes a dramatic 88% decrease in absorbance, confirming its potent hemolytic activity. At low API concentrations (1.562 μM), hemolysis remains negligible. However, slight hemolysis becomes noticeable at concentrations ranging from 3.125 μM to 50 μM ($p < 0.01$), with absorbance reductions of approximately 13–14%, except for 6.25 μM, which shows a slightly higher reduction of 16% ($p < 0.001$). At concentrations ≥ 100 μM, hemolysis becomes insignificant. These findings suggest that API induces minor hemolysis at lower concentrations but maintains erythrocyte stability at concentrations ≥ 100 μM.

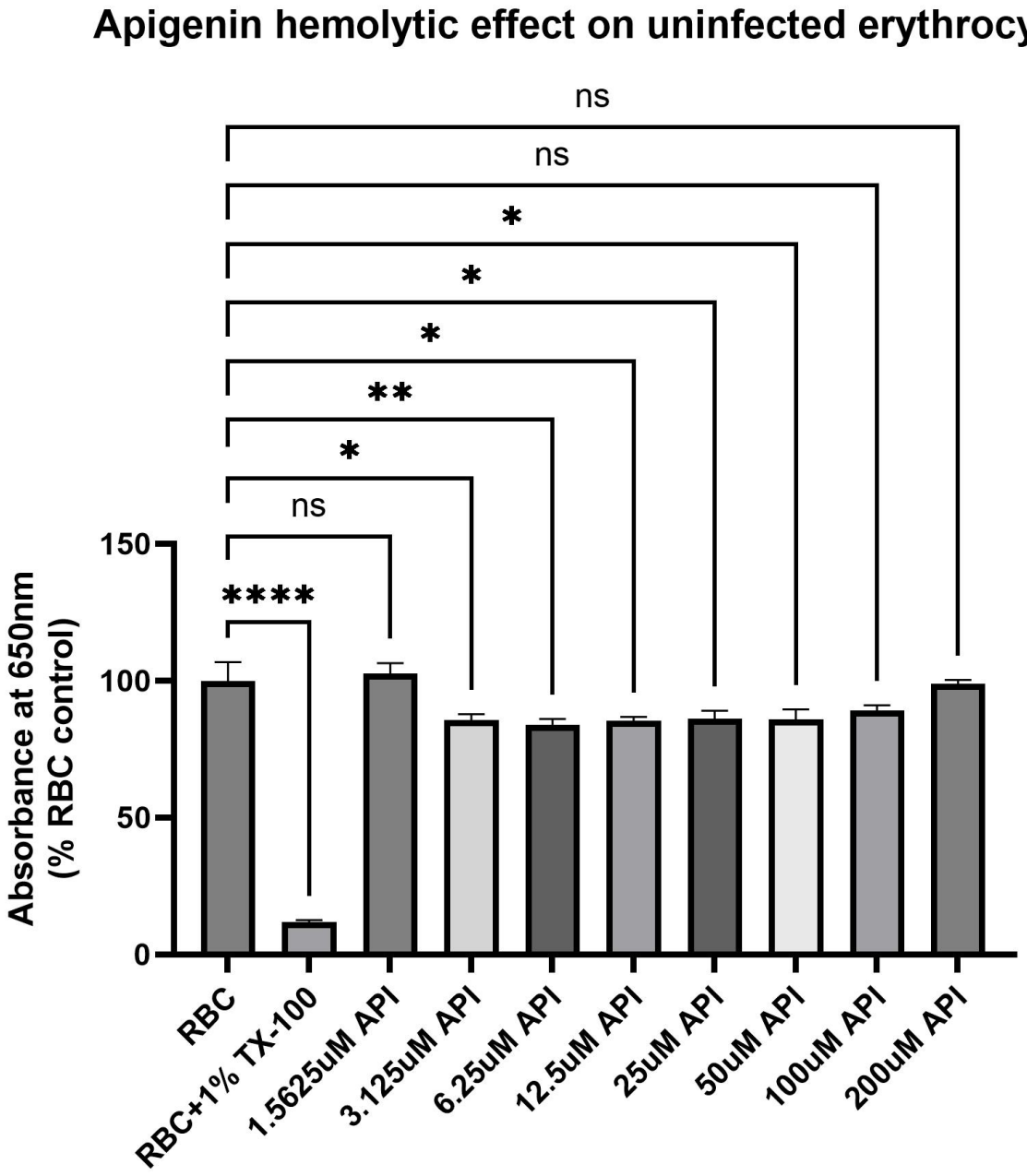

Figure 9. Hemolytic effect of apigenin (API) on uninfected erythrocytes. Erythrocytes were incubated in RPMI 1640 medium without phenol red for 24 hours at 37°C with increasing concentrations (μM) of API. Hemolytic activity was evaluated by comparing cell density, measured as absorbance at 650 nm. Results are expressed as mean absorbance values relative to the RBC control. Error bars represent ± S.D. from two independent experiments performed in triplicate. Statistically significant differences compared to the control are indicated by *($p < 0.01$), **($p < 0.001$) and ****($p < 0.0001$), while nonsignificant differences are labeled "ns".

4.3 Effects of Sulfasalazine on Uninfected Erythrocytes

Similarly, the effects of SSZ on ROS levels and hemolysis were evaluated in erythrocytes incubated with increasing concentrations of SSZ for 24 hours.

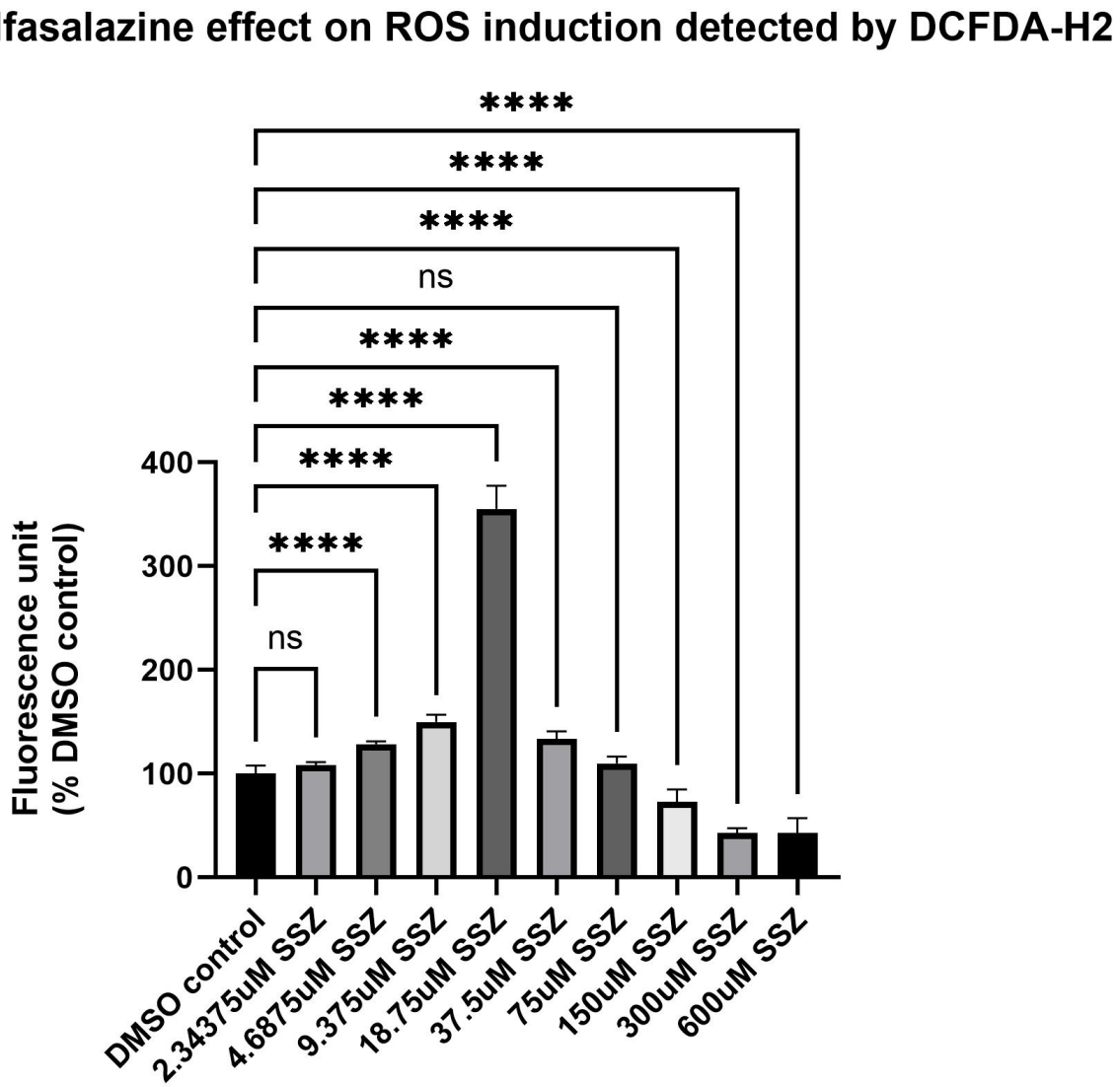

Figure 10. The effect of sulfasalazine (SSZ) on intracellular ROS levels in uninfected erythrocytes. Erythrocytes were incubated in RPMI 1640 medium without phenol red for 24 hours at 37°C with increasing concentrations (μM) of SSZ. Intracellular ROS levels were measured using 10 μM of the fluorescent probe H_2DCFDA. Results are presented as the mean fluorescence values relative to the DMSO control. Error bars represent ± S.D. of two independent experiments performed in triplicate. Statistically significant differences are denoted by ****($p < 0.0001$), while nonsignificant differences are labeled "ns".

Figure 10 illustrates that SSZ induces a dose-dependent increase in ROS levels, peaking at 18.75 μM with a substantial 255% rise in ROS compared to the DMSO control (****$p < 0.0001$). Lower concentrations, such as 4.8675 μM and 9.375 μM, elevated ROS levels by 28% and 50%, respectively. Significant differences emerged between concentrations, including a 227% increase in ROS at 18.75 μM relative to 4.8675 μM (****$p < 0.0001$). Furthermore, 18.75 μM doubled ROS levels compared to 9.375 μM (****$p < 0.0001$). From 37.5 μM onward, ROS levels declined, forming a bell-shaped dose-response curve. While 37.5 μM and 75 μM still enhanced ROS levels by 33% and 10%, respectively, compared to the DMSO control, these increases were significantly lower than those at 18.75 μM. Higher concentrations (150 μM, 300 μM, and 600 μM) progressively reduced ROS levels by 27%, 57.3%, and 57.1%, respectively, compared to the DMSO control (****$p < 0.0001$). These findings suggest a biphasic response where low concentrations of SSZ stimulate ROS production, whereas high concentrations may suppress ROS levels due to cytotoxic effects or ROS-scavenging mechanisms.

Figure 11 presents the hemolytic effects of SSZ on uninfected erythrocytes after 24 hours of incubation at 37°C. At 6.25 μM SSZ, hemolysis is negligible (ns). Between 12.5 μM and 50 μM, a slight reduction in absorbance is observed, ranging from 10–12% (*$p < 0.01$). At concentrations of 100 μM and above, the reduction in absorbance decreases, with 100 μM, 200 μM, and 400 μM showing reductions of 8% (*$p < 0.01$), 6% (*$p < 0.01$), and 1.5% (ns), respectively. Notably, 800 μM SSZ unexpectedly increases absorbance by 18%. Most comparisons between SSZ concentrations show insignificant differences or are limited to *$p < 0.01$, indicating the absence of a dose-dependent relationship between SSZ and hemolysis.

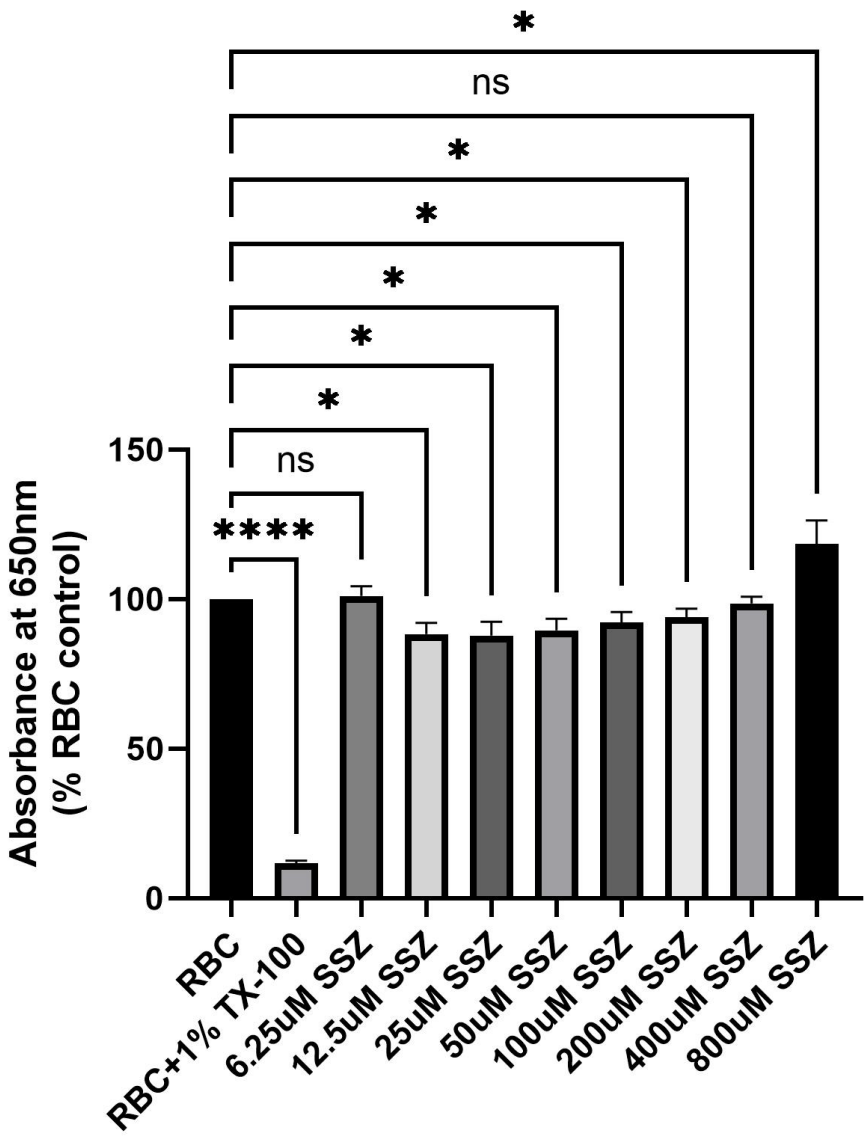

Figure 11. Hemolytic effect of sulfasalazine (SSZ) on uninfected erythrocytes. Erythrocytes were incubated in RPMI 1640 medium without phenol red for 24 hours at 37°C with increasing concentrations (μM) of SSZ. Hemolytic activity was evaluated by comparing cell density, measured as absorbance at 650 nm. Results are expressed as mean absorbance values relative to the RBC control. Error bars represent ± S.D. from two independent experiments performed in triplicate. Statistically significant differences compared to the control are indicated by *($p < 0.01$) and ****($p < 0.0001$), while nonsignificant differences are labeled "ns".

4.4 Effects of Sulfasalazine Combined with Apigenin on uninfected erythrocytes

Having established that both API and SSZ induce ROS in erythrocytes, the combined effects of these compounds were evaluated to determine whether their combination could reduce the effective concentrations needed to induce ROS. Erythrocytes were incubated with increasing concentrations of SSZ, either alone or in combination with 12.5 μM or 25 μM API, for 24 hours. The results in Figure 12 indicate that API enhances ROS generation when combined with specific concentrations of SSZ. At 4.8675 μM SSZ, adding 12.5 μM or 25 μM API significantly increases ROS levels by 68% and 67%, respectively (*$p < 0.01$) compared to SSZ alone. At 9.375 μM SSZ, combining 12.5 μM API results in a 107% increase (***$p < 0.0001$), while 25 μM API induces an 86% increase (**$p < 0.001$). In contrast, at 18.75 μM SSZ, both API concentrations significantly decrease ROS levels, with reductions of 125% (12.5 μM API) and 144% (25 μM API) (****$p < 0.0001$).

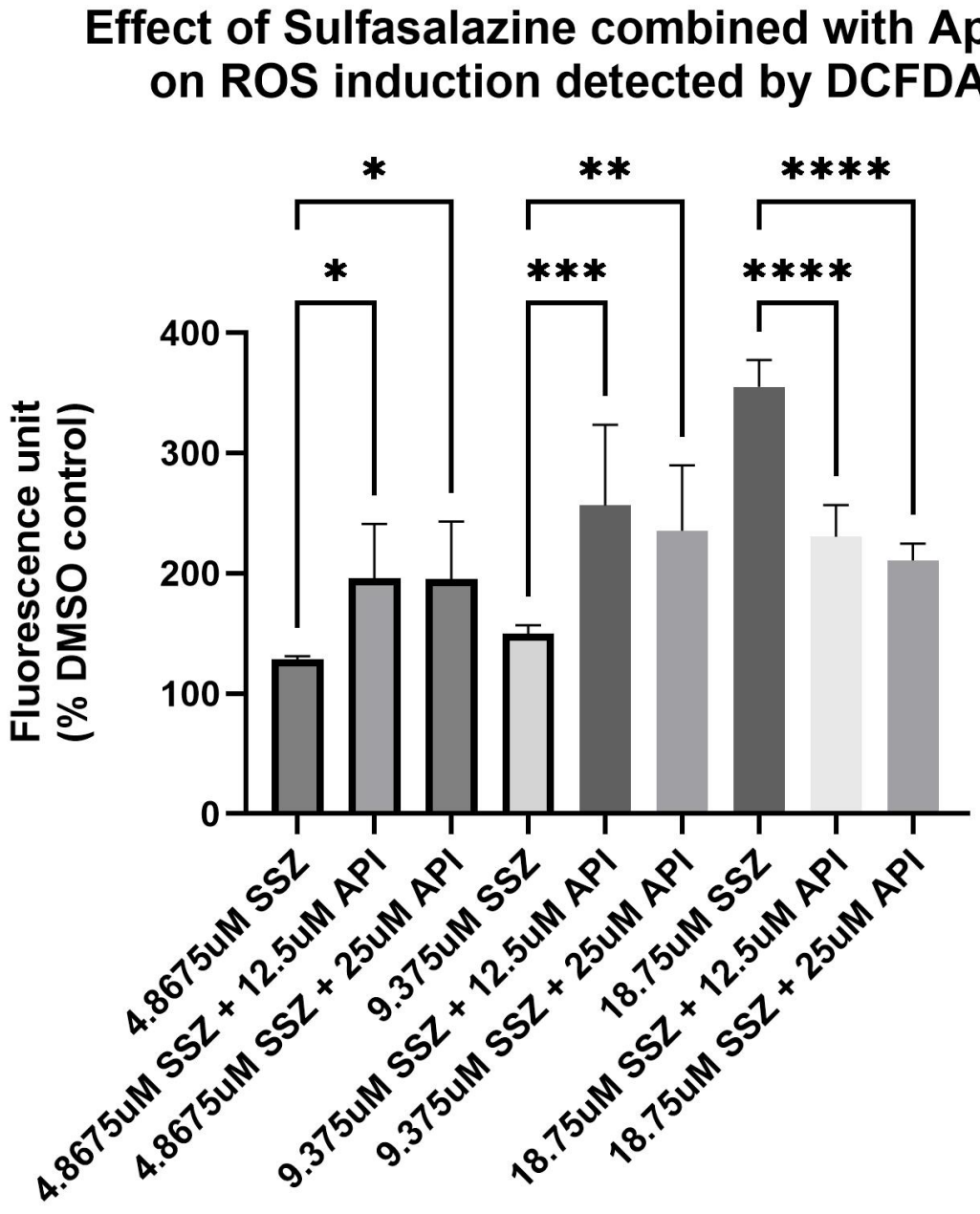

Figure 12. The effect of sulfasalazine (SSZ) combined with apigenin (API) on intracellular ROS levels in uninfected erythrocytes. Erythrocytes were incubated in RPMI 1640 medium without phenol red for 24 hours at 37°C with increasing concentrations of SSZ (μM) alone or combined with either 12.5 μM or 25 μM API. Intracellular ROS levels were measured using 10 μM of the fluorescent probe H_2DCFDA. Results are expressed as mean fluorescence values relative to the DMSO control. Error bars represent ± S.D. from two independent experiments performed in triplicate. Statistically significant differences are indicated by *($p < 0.01$), **($p < 0.001$), *** ($p = 0.0003$) and **** ($p<0.0001$), while nonsignificant differences are labeled "ns".

Figure 13 depicts the hemolytic effects of SSZ combined with 3.125 μM API on uninfected erythrocytes. No significant hemolysis occurred at SSZ concentrations up to 50 μM. At 100 μM, 200 μM, and 400 μM SSZ, minor hemolysis was observed, with absorbance reductions of 16%, 15%, and 13%, respectively (*$p < 0.01$). At 800 μM SSZ, absorbance increased by 13% compared to the RBC control.

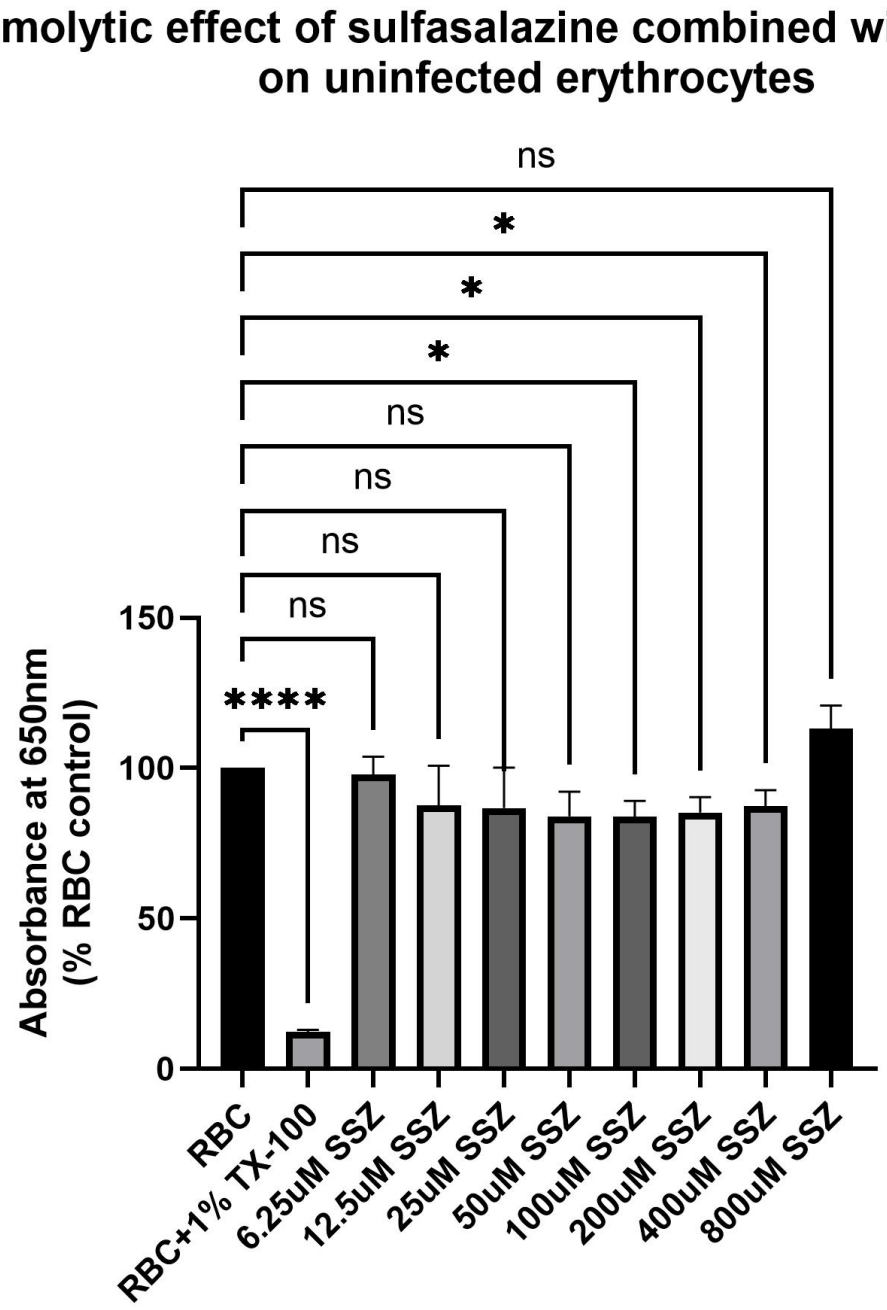

Figure 13. Hemolytic effect of sulfasalazine (SSZ) combined with apigenin (API) on uninfected erythrocytes. Erythrocytes were incubated in RPMI 1640 medium without phenol red for 24 hours at 37°C with increasing concentrations (μM) of SSZ combined with 3.125 μM API. Hemolytic activity was evaluated by comparing cell density, measured as absorbance at 650 nm. Results are expressed as mean absorbance values relative to the RBC control. Error bars represent ± S.D. from two independent experiments performed in triplicate. Statistically significant differences compared to the control are indicated by *($p < 0.01$) and ****($p < 0.0001$), while nonsignificant differences are labeled "ns".

4.5 Effects of API and SSZ, Alone or in Combination, on the Proliferation of *Plasmodium falciparum*

Having established that API and SSZ, alone or in combination, induce ROS in uninfected erythrocytes, their effects on *P. falciparum* were evaluated using the SYBR Green I®-based parasite growth inhibition assay.

Figure 14 illustrates the inhibitory effects of API on the proliferation of *P. falciparum* strains, including CQ-sensitive (3D7) and CQ-resistant (Dd2). API reduces parasite proliferation in a dose-dependent manner, with increasing concentrations of API (0–100 μM) leading to a progressive decline in proliferation. 3D7 and Dd2 strains exhibit similar sensitivity to API, as their inhibition curves closely align, indicating comparable efficacy against CQ-sensitive and CQ-resistant strains. At the highest tested concentration (100 μM API), parasite proliferation approaches 0%, reflecting complete inhibition of growth. The IC50 values, representing the concentrations required to reduce parasite proliferation by 50% relative to the positive control, are 7.386 μM for 3D7 (95% confidence interval [CI]: 6.545–8.324 μM) and 9.090 μM for Dd2 (95% CI: 7.675–10.73 μM).

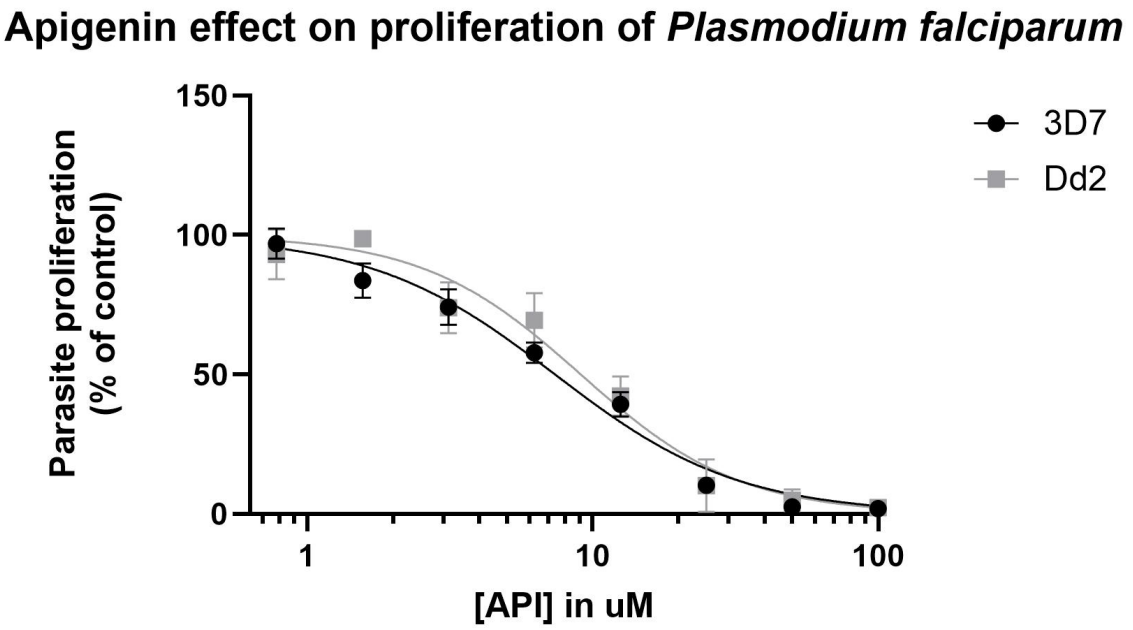

Figure 14. Effect of apigenin (API) on the proliferation of *Plasmodium falciparum*. CQ-sensitive (3D7) and CQ-resistant (Dd2) strains of *P. falciparum* were cultured in vitro with increasing concentrations of API (0–100 μM) or without API (positive control). Uninfected erythrocytes served as the negative control, and their background signal was subtracted from both the positive control and test samples. Results are presented as the mean percentage of parasite proliferation relative to the positive control. Error bars represent ± S.D. from three independent experiments performed in triplicate.

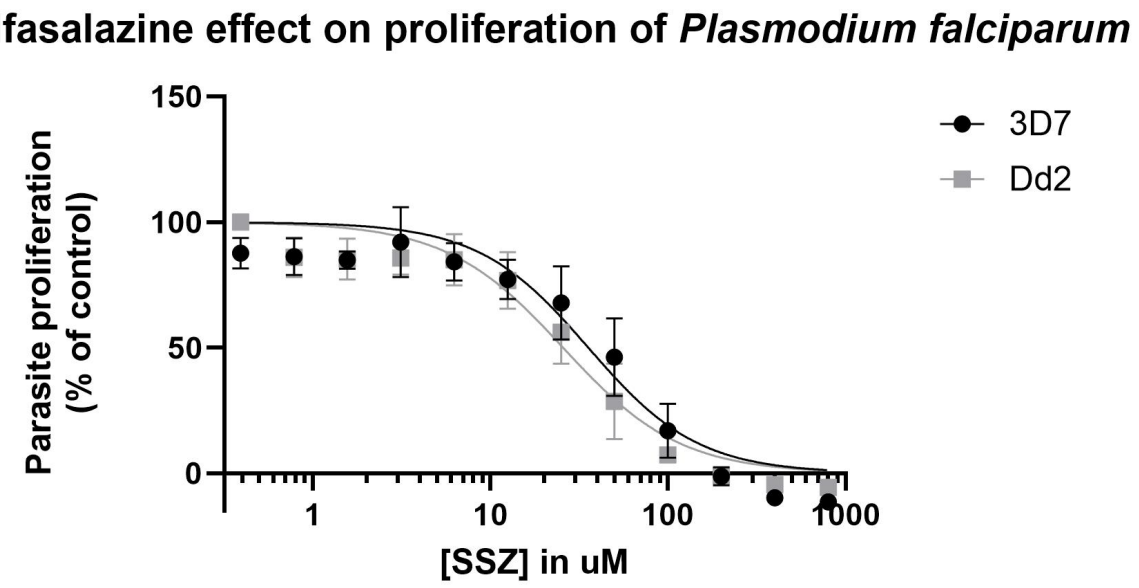

Figure 15. Effect of sulfasalazine (SSZ) on the proliferation of *Plasmodium falciparum*. CQ-sensitive (3D7) and CQ-resistant (Dd2) strains of *P. falciparum* were cultured in vitro with increasing concentrations of SSZ (0–800 μM) or without SSZ (positive control). Uninfected erythrocytes served as the negative control, and their background signal was subtracted from both the positive control and test samples. Results are presented as the mean percentage of parasite proliferation relative to the positive control. Error bars represent ± S.D. from three independent experiments performed in triplicate.

Similarly, Figure 15 illustrates the dose-dependent inhibitory effect of SSZ on the proliferation of 3D7 and Dd2. Increasing SSZ concentrations (0–800 μM) progressively reduce parasite proliferation, with both strains showing comparable sensitivity. At the highest tested concentration (800 μM), near-complete growth inhibition is observed. The IC50 values for SSZ are 35.65 μM for 3D7 (95% CI: 26.86–46.34 μM) and 25.69 μM for Dd2 (95% CI: 20.07–32.47 μM).

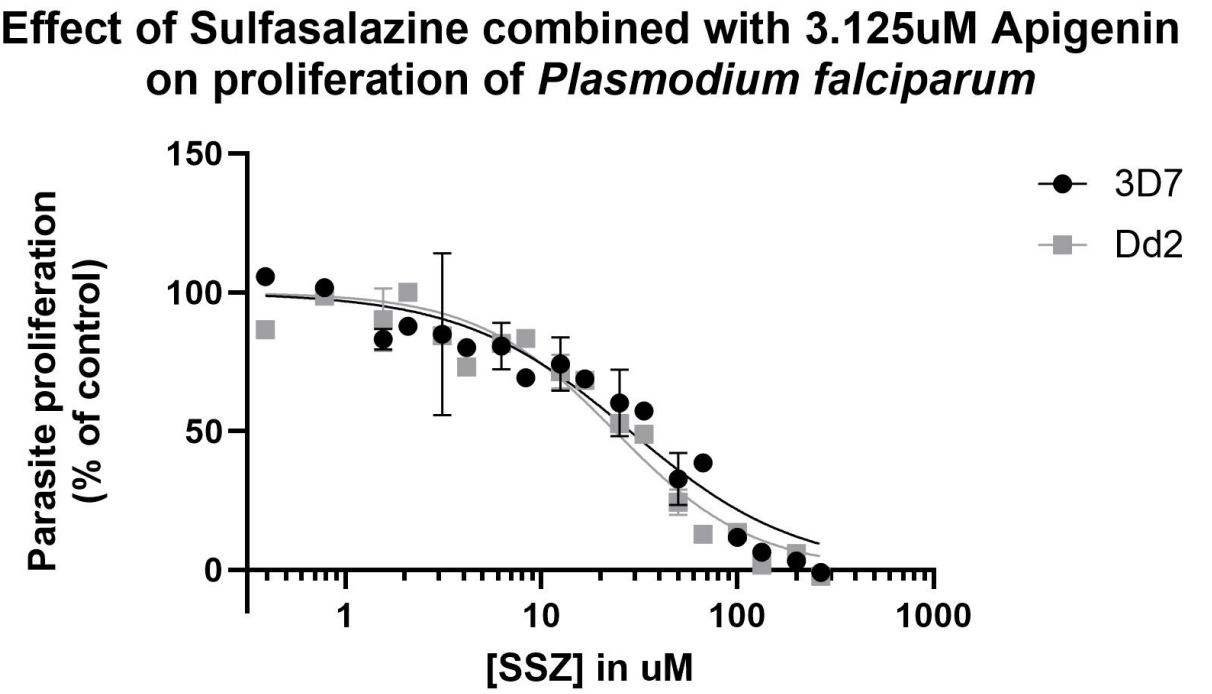

Figure 16. Effect of sulfasalazine (SSZ) combined with apigenin (API) on the proliferation of *Plasmodium falciparum*. CQ-sensitive (3D7) and CQ-resistant (Dd2) strains of *P. falciparum* were cultured *in vitro* with increasing concentrations of SSZ (0–266.7 μM) combined with 3.125 μM API. Cultures without any compounds served as the positive control, while uninfected erythrocytes served as the negative control, with their background signal subtracted from all samples. Results are expressed as the mean percentage of parasite proliferation relative to the positive control. Error bars represent ± S.D. from three independent experiments performed in triplicate.

Figure 16 illustrates the dose-dependent inhibitory effect of combining SSZ (0–266.7 μM) with 3.125 μM API on the proliferation of *Plasmodium falciparum* strains 3D7 and Dd2, which exhibit comparable sensitivity. The IC50 values for the combination treatment are 28.3 μM for 3D7 (95% CI: 21.44–37.32 μM) and 23.72 μM for Dd2 (95% CI: 19.88–28.23 μM).

5 DISCUSSION

Malaria, caused by *Plasmodium* parasites, remains a global health crisis, with drug resistance posing critical challenges. A previous study in our lab showed that API at 25 μM and 50 μM increased ROS by enhancing ABCC1 efflux activity, depleting GSH, and significantly inhibiting *P. falciparum* proliferation, with IC50 values of 36.02 ± 2.4 μM (3D7) and 34.45 ± 2.4 μM (Dd2) [62]. This study builds on these findings by exploring API's effects on ROS induction and parasite inhibition, both alone and combined with SSZ, hypothesized to induce ROS as it was proven to limit cysteine availability for GSH synthesis [56]. Additionally, their hemolytic activity in uninfected erythrocytes was assessed to determine their potential as suitable antimalarial agents.

Before evaluating the effects of these compounds, this study investigated the impact of their solvent, dimethyl sulfoxide (DMSO), which has been reported to modulate ROS levels by acting as either an oxidant or antioxidant depending on its concentration [72]. Research indicates that DMSO concentrations between 1% and 14% (% v/v) can reduce oxidative damage but exhibit cytotoxic effects at levels ≥1% across various cell types [72]. Specifically in erythrocytes, DMSO stiffens membranes at 1%, softens them at higher concentrations (5–10%), and increases membrane permeability to ATP at concentrations ≥3% [73]. Consistent with these findings, this study demonstrated that DMSO concentrations >2% significantly reduced ROS levels but induced hemolysis at 4.5% and 9%. The observed reduction in ROS at higher DMSO concentrations (>4%) may result from cytotoxicity, which disrupts intracellular esterase activity required to cleave and activate the ROS detection probe H_2DCFDA.

After eliminating potential DMSO effects, this study confirmed prior findings, showing that 25 μM and 50 μM API significantly increased ROS levels, with 50 μM doubling ROS and 12.5 μM inducing a 40% rise. While these concentrations exhibited slight hemolytic activity ($p < 0.01$), no hemolysis was observed at 1.5625 μM or the two highest concentrations tested (100 μM and 200 μM). Similarly, a study by Coralie Boulet et al. reported no significant hemolytic or eryptotic effects of API at concentrations up to 10 μM [74]. The observed hemolysis at API concentrations between 3.125 μM and 50 μM may reflect uneven cell distribution. Erythrocytes were prepared in large volumes as stock solutions and aliquoted into sterile cell culture-treated petri dishes for subsequent transfer to a 96-well plate. Despite manual orbital shaking to homogenize the erythrocyte suspension, the method may not have achieved uniform distribution. Given that API induces ROS in a dose-dependent manner, its cytotoxicity should also correlate with dose; however, the absence of hemolysis at the lowest and the two highest concentrations tested suggests other contributing factors to the hemolysis observed at lower doses.

Interestingly, the IC50 values of API in this study (7.386 ± 0.9 μM for 3D7 and 9.090 ± 1.5 μM for Dd2) were markedly lower than those reported in previous research (36.02 ± 2.4 μM for 3D7 and 34.45 ± 2.4 μM for Dd2). The study by Coralie Boulet et al. also investigated API's effects on inhibiting 3D7 proliferation, reporting a much higher IC50 of 65.78 μM. Despite all studies employing a similar protocol using SYBR-based detection (with Coralie Boulet et al. using SYBR Gold instead of SYBR Green [74]), the discrepancies in IC50 values may stem from differences in drug preparation and other factors such as differences in source and age of erythrocytes or ABCC1 expression levels. The Coralie Boulet et al. group used 0.5% v/v DMSO for drug preparation [74], whereas this study used 0.2%. As previously discussed, low concentrations of DMSO protect against ROS, and given that the parasite proliferation assay

requires a longer incubation time (72 hours), the DMSO effect might have a more pronounced influence on the IC50. Considering 12.5 μM API significantly increased ROS in uninfected erythrocytes, the lower IC50s obtained in this study support the hypothesis that *P. falciparum* infection exacerbates oxidative stress in erythrocytes and further ROS induction via API contributes to parasite clearance.

Regarding SSZ, limited research has examined its impact on ROS levels in erythrocytes, with most studies focusing on its ROS-inducing effects in cancer cells at concentrations between 0.2 mM and 1 mM [75-78]. To bridge this gap, this study investigated SSZ's ability to modulate ROS levels in erythrocytes over a concentration range of 2 μM to 600 μM. Interestingly, SSZ displayed a biphasic dose-response curve, as shown in Figure 3a, characterized by a bell-shaped profile. Lower SSZ concentrations (4.8675 μM to 18.75 μM) significantly stimulated ROS production, peaking at 18.75 μM with a 255% increase (****$p < 0.0001$). Higher concentrations (75 μM and above) progressively reduced ROS levels, with 300 μM and 600 μM both showing a 57% decrease compared to the DMSO control.

This ROS reduction was initially attributed to cytotoxicity, similar to the effects observed with 9% DMSO, where a reduction in cell count lowered the detectable fluorescence signal. However, hemolytic assays for SSZ showed no evidence of severe lysis, particularly at 400 μM, where cell density remained comparable to the DMSO control. Previous study has shown that SSZ and its metabolites, such as 5-aminosalicylic acid (5-ASA) and sulfapyridine, scavenge free radicals [79]. In another study, SSZ at 300 μM reduced oxidative stress in high-glucose vessels by activating antioxidant enzymes like heme oxygenase-1 [80]. Additionally, nanozymes with SSZ (Sul-MPBs) developed to treat inflammatory bowel disease (IBD) in a mouse model

effectively scavenged ROS, neutralized hydrogen peroxide (H_2O_2), and mimicked the activities of antioxidant enzymes, including CAT, SOD, and GPx [81]. Thus, the ROS reduction observed at higher SSZ concentrations in this study may result from its ROS-scavenging capabilities, while lower concentrations likely inhibit system xCT, limiting cysteine availability and enhancing ROS production.

For inhibiting *Plasmodium* proliferation, SSZ exhibits IC50 values ranging from 27 μM to 46 μM for 3D7 and 20 μM to 32 μM for Dd2. Unlike API, whose IC50 values fall below the concentrations required for significant ROS induction, SSZ's IC50s correspond to its peak ROS induction concentration (18.75 μM) and the onset of ROS decline at 37.5 μM. While lower concentrations such as 4.8675 μM and 9.375 μM significantly induced ROS, the IC50s of SSZ were expected to be lower. However, since infection exacerbates oxidative stress and can trigger post-translational modifications of erythroid proteins [82], these alterations may have influenced the interactions between SSZ and its target system xCT, necessitating slightly higher concentrations for effective inhibition.

When combined with 12.5 μM or 25 μM API, SSZ at 4.8675 μM and 9.375 μM exhibited additive effects on ROS induction, with 9.375 μM producing a more pronounced increase, and 12.5 μM API showing greater efficacy. However, at 18.75 μM SSZ, the combination with API reduced ROS levels, suggesting that API may exhibit antioxidant properties under these conditions. Studies have shown that API's antioxidant activity arises from its ability to scavenge ROS at specific structural sites and regulate the activity of key oxidative enzymes, including cyclooxygenase (COX-2), NOS, XO, nitric oxide (NO), and lipoxygenase (LOX) [83]. Interestingly, many phytochemicals, including luteolin, a close chemical relative of API, exhibit hormetic behaviour, producing opposite biological effects depending on the dose: low doses

often stimulate biological responses, while higher doses inhibit them [84-85]. The reduction in ROS at 18.75 μM SSZ combined with API may result from saturation, as this concentration represents the peak of ROS induction by SSZ, allowing API's antioxidant properties to dominate. This interpretation is supported by the minimal hemolysis observed in the combination treatment. Furthermore, API's potential hormetic behaviour might explain why combining 3.125 μM API, selected as 50% of its IC50 value, with SSZ failed to significantly lower SSZ's IC50.

When comparing the 95% confidence intervals (CI) of the IC50 values for API, SSZ, and the combination treatment, a noticeable increase in the interval was observed when using SSZ. The 95% CI for API was approximately ± 0.9 μM for 3D7 and ± 1.5 μM for Dd2, reflecting the high sensitivity and accuracy of the SYBR Green I®-based parasite growth inhibition assay. In contrast, the 95% CI for SSZ increased to around ± 10 μM for 3D7 and ± 6 μM for Dd2 when used alone, and approximately ± 8 μM for 3D7 and ± 4 μM for Dd2 when combined with API. Given the demonstrated efficacy of the SYBR Green I® assay with CQ controls (results not shown), this increased variability may be associated with differing expression levels of system xCT in erythrocytes, a factor not explored in this study.

Another limitation of this study is its exclusive focus on hemolysis (i.e., necrosis) as a cytotoxic outcome, without addressing eryptosis, an alternative mechanism of erythrocyte death frequently linked to ROS overproduction [86]. Eryptosis occurs in response to stimuli that surpass the cell's survival threshold but are not menacing enough to cause hemolysis [86]. Unlike hemolysis, eryptosis involves cell shrinkage rather than rupture and is marked by the externalization of phosphatidylserine (PS) on the cell membrane, signalling macrophages for clearance [86]. Considering that most hemolytic assay results indicated minimal lysis, evaluating eryptosis using fluorescently labelled Annexin V, which binds with high affinity to PS, and

analyzing it through flow cytometry could offer a more comprehensive understanding of how the tested compounds affect erythrocyte viability [87].

CONCLUSION

This study aimed to explore the therapeutic potential of targeting host erythrocytes as an alternative strategy to combat malaria by disrupting redox homeostasis through modulation of GSH levels. A significant advantage of this approach lies in its reduced likelihood of inducing drug resistance in parasites, as the pathogens are not directly targeted. The findings revealed that both API and SSZ effectively induced ROS in a dose-dependent manner, leading to oxidative stress that selectively inhibited the proliferation of both CQ-sensitive (3D7) and CQ-resistant (Dd2) *Plasmodium falciparum* strains. Minimal hemolysis was observed at therapeutic concentrations. However, the combination of API and SSZ did not significantly enhance parasite clearance beyond their individual effects, suggesting opportunities for further optimization in combination therapy.

The study also highlighted the hormetic or biphasic behavior of API and SSZ, which act as ROS inducers at lower concentrations and exhibit potential antioxidant effects at higher concentrations. These findings underscore the importance of investigating the mechanisms underlying these responses, including the activities of erythrocyte transporters such as ABCC1 and system xc^- under stress conditions, as well as the potential for eryptosis as an alternative mode of erythrocyte death.

The limitations of this study, including its focus on hemolysis as the primary cytotoxic outcome and the variability observed in SSZ's IC50 values, highlight the need for more comprehensive analyses. Future studies should incorporate assessments of eryptosis using tools such as Annexin V-based flow cytometry to better understand the impact of these compounds on erythrocyte viability. Additionally, exploring the potential of combination therapies with other antimalarial agents and evaluating their in vivo efficacy will be crucial for advancing these findings toward clinical application.

In conclusion, this study provides evidence that targeting host antioxidative systems through modulation of GSH levels represents a promising strategy for antimalarial chemotherapy. By inducing oxidative stress in infected erythrocytes while sparing uninfected cells, API and SSZ offer a novel therapeutic avenue that could complement existing malaria treatments and address the growing challenge of drug resistance.

REFERENCES

[1] M. Dagen, Chapter 1 - History of malaria and its treatment, in: G.L. Patrick (Ed.), Antimalarial Agents, Elsevier, 2020: pp. 1–48. https://doi.org/10.1016/B978-0-08-101210-9.00001-9.

[2] J.E. Mertens, A History of Malaria and Conflict, Parasitol Res 123 (2024) 165. https://doi.org/10.1007/s00436-024-08167-4.

[3] S. Rai, Omkar, G. Mishra, Silent Architects: The Mosquitoes, in: Omkar (Ed.), Mosquitoes: Biology, Pathogenicity and Management, Springer Nature, Singapore, 2024: pp. 1–22. https://doi.org/10.1007/978-981-97-4163-2_1.

[4] O. Simonetti, C. Contini, M. Martini, The history of Gin and Tonic; the infectious disease specialist long drink. When gin and tonic was not ordered but prescribed, Infez Med 30 (2022) 619–626. https://doi.org/10.53854/liim-3004-18.

[5] World Health Organization. World malaria report 2023. Geneva: World Health Organization; 2023. [Accessed 2024 Dec 3]. Available from: https://www.who.int/publications/i/item/9789240086173

[6] S. Sato, Plasmodium-a brief introduction to the parasites causing human malaria and their basic biology, J Physiol Anthropol 40 (2021) 1. https://doi.org/10.1186/s40101-020-00251-9.

[7] R.N. Price, R.J. Commons, K.E. Battle, K. Thriemer, K. Mendis, Plasmodium vivax in the Era of the Shrinking P. falciparum Map, Trends in Parasitology 36 (2020) 560–570. https://doi.org/10.1016/j.pt.2020.03.009.

[8] M. Fikadu, E. Ashenafi, Malaria: An Overview, Infect Drug Resist 16 (2023) 3339–3347. https://doi.org/10.2147/IDR.S405668.

[9] K. Wu, Malaria Parasites: Species, Life Cycle, and Morphology, in: H. Mehlhorn, J. Li, K. Wu (Eds.), Malaria Control and Elimination in China: A Successful Guide from Bench to Bedside, Springer International Publishing, Cham, 2023: pp. 49–69. https://doi.org/10.1007/978-3-031-32902-9_4.

[10] Â.F. Chora, M.M. Mota, M. Prudêncio, The reciprocal influence of the liver and blood stages of the malaria parasite's life cycle, International Journal for Parasitology 52 (2022) 711–715. https://doi.org/10.1016/j.ijpara.2022.02.002.

[11] Franklyn Ohiagu, Paul Chikezie, Clinton Ahaneku, Chinwendu Chikezie, Favour Law-Obi, Pathophysiology of Severe Malaria Infection, AJHS 7 (2021). https://doi.org/10.15419/ajhs.v7i2.492.

[12] K.R. Dobbs, J.N. Crabtree, A.E. Dent, Innate immunity to malaria—The role of monocytes, Immunological Reviews 293 (2020) 8–24. https://doi.org/10.1111/imr.12830.

[13] R. Varo, C. Chaccour, Q. Bassat, Update on malaria, Medicina Clínica 155 (2020) 395–402. https://doi.org/10.1016/j.medcli.2020.05.010.

[14] CDC, Symptoms of Malaria, Malaria (2024). https://www.cdc.gov/malaria/symptoms/index.html (accessed December 4, 2024).

[15] M.F. Wiser, Knobs, Adhesion, and Severe Falciparum Malaria, Trop Med Infect Dis 8 (2023) 353. https://doi.org/10.3390/tropicalmed8070353.

[16] V. Djokic, S.C. Rocha, N. Parveen, Lessons Learned for Pathogenesis, Immunology, and Disease of Erythrocytic Parasites: Plasmodium and Babesia, Frontiers in Cellular and Infection Microbiology 11 (2021). https://www.frontiersin.org/journals/cellular-and-infection-microbiology/articles/10.3389/fcimb.2021.685239.

[17] L.E. Fitri, T. Widaningrum, A.T. Endharti, M.H. Prabowo, N. Winaris, R.Y.B. Nugraha, Malaria diagnostic update: From conventional to advanced method, Journal of Clinical Laboratory Analysis 36 (2022) e24314. https://doi.org/10.1002/jcla.24314.

[18] M.A. Shibeshi, Z.D. Kifle, S.A. Atnafie, Antimalarial drug resistance and novel targets for antimalarial drug discovery, Infect. Drug Resist. 13 (2020) 4047–4060. https://doi.org/10.2147/IDR.S279433.

[19] M.W. Irvine, Chapter 5 - Agents acting on pyrimidine metabolism, in: G.L. Patrick (Ed.), Antimalarial Agents, Elsevier, 2020: pp. 133–185. https://doi.org/10.1016/B978-0-08-101210-9.00005-6.

[20] Pethrak Chatpong, Posayapisit Navaporn, Pengon Jutharat, Suwanakitti Nattida, Saeung Atiporn, Shorum Molnipha, Aupalee Kittipat, Taai Kritsana, Yuthavong Yongyuth, Kamchonwongpaisan Sumalee, Jupatanakul Natapong, New Insights into Antimalarial Chemopreventive Activity of Antifolates, Antimicrobial Agents and Chemotherapy 66 (2022) e01538-21. https://doi.org/10.1128/aac.01538-21.

[21] S.L. Rawe, Chapter 4 - Artemisinin and artemisinin-related agents, in: G.L. Patrick (Ed.), Antimalarial Agents, Elsevier, 2020: pp. 99–132. https://doi.org/10.1016/B978-0-08-101210-9.00004-4.

[22] N. Erhunse, D. Sahal, Protecting future antimalarials from the trap of resistance: Lessons from artemisinin-based combination therapy (ACT) failures, Journal of Pharmaceutical Analysis 11 (2021) 541–554. https://doi.org/10.1016/j.jpha.2020.07.005.

[23] R.W. van der Pluijm, C. Amaratunga, M. Dhorda, A.M. Dondorp, Triple Artemisinin-Based Combination Therapies for Malaria – A New Paradigm?, Trends in Parasitology 37 (2021) 15–24. https://doi.org/10.1016/j.pt.2020.09.011.

[24] A. Arya, L.P. Kojom Foko, S. Chaudhry, A. Sharma, V. Singh, Artemisinin-based combination therapy (ACT) and drug resistance molecular markers: A systematic review of clinical studies from two malaria endemic regions – India and sub-Saharan Africa, International Journal for Parasitology: Drugs and Drug Resistance 15 (2021) 43–56. https://doi.org/10.1016/j.ijpddr.2020.11.006.

[25] C. Rodrigo, S. Rajapakse, S.D. Fernando, Compliance with primary malaria chemoprophylaxis: Is weekly prophylaxis better than daily prophylaxis?, Patient Prefer. Adherence 14 (2020) 2215–2223. https://doi.org/10.2147/PPA.S255561.

[26] E. DeVos, N. Dunn, Malaria prophylaxis, in: StatPearls, StatPearls Publishing, Treasure Island (FL), 2024. https://www.ncbi.nlm.nih.gov/books/NBK551639/ (accessed December 6, 2024).

[27] CDC, Preventing Malaria While Traveling, Malaria (2024). https://www.cdc.gov/malaria/prevention/index.html (accessed December 4, 2024).

[28] Malaria | CDC Yellow Book 2024, (n.d.). https://wwwnc.cdc.gov/travel/yellowbook/2024/infections-diseases/malaria (accessed December 4, 2024).

[29] E.B. Esu, C. Oringanje, M.M. Meremikwu, Intermittent preventive treatment for malaria in infants, Cochrane Database Syst. Rev. 7 (2021) CD011525. https://doi.org/10.1002/14651858.CD011525.pub3.

[30] J. Thwing, J. Williamson, I. Cavros, J.R. Gutman, Systematic review and meta-analysis of seasonal malaria chemoprevention, Am. J. Trop. Med. Hyg. 110 (2024) 20–31. https://doi.org/10.4269/ajtmh.23-0481.

[31] Z.D. Schneider, M.P. Shah, M.C. Boily, A.L. Busbee, J. Hwang, K.A. Lindblade, J.R. Gutman, Mass drug administration to reduce malaria transmission: A systematic review and meta-analysis, Am. J. Trop. Med. Hyg. 110 (2024) 17–29. https://doi.org/10.4269/ajtmh.22-0766.

[32] Malaria vaccine: WHO position paper – May 2024, (n.d.). https://www.who.int/publications/i/item/who-wer-9919-225-248 (accessed December 4, 2024).

[33] WHO guidelines for malaria, (n.d.). https://www.who.int/publications/i/item/guidelines-for-malaria (accessed December 4, 2024).

[34] T.M. Schäfer, L. Pessanha de Carvalho, J. Inoue, A. Kreidenweiss, J. Held, The problem of antimalarial resistance and its implications for drug discovery, Expert Opinion on Drug Discovery 19 (2024) 209–224. https://doi.org/10.1080/17460441.2023.2284820.

[35] S.L. Rawe, C. McDonnell, Chapter 3 - The cinchona alkaloids and the aminoquinolines, in: G.L. Patrick (Ed.), Antimalarial Agents, Elsevier, 2020: pp. 65–98. https://doi.org/10.1016/B978-0-08-101210-9.00003-2

[36] S.H. Shafik, S.N. Richards, B. Corry, R.E. Martin, Mechanistic basis for multidrug resistance and collateral drug sensitivity conferred to the malaria parasite by polymorphisms in

PfMDR1 and PfCRT, PLOS Biology 20 (2022) e3001616. https://doi.org/10.1371/journal.pbio.3001616.

[37] C. Rasmussen, P. Alonso, P. Ringwald, Current and emerging strategies to combat antimalarial resistance, Expert Review of Anti-Infective Therapy 20 (2022) 353–372. https://doi.org/10.1080/14787210.2021.1962291.

[38] B. Hanboonkunupakarn, N.J. White, Advances and roadblocks in the treatment of malaria, British Journal of Clinical Pharmacology 88 (2022) 374–382. https://doi.org/10.1111/bcp.14474.

[39] M. Kucharski, S. Nayak, M. Gendrot, A.M. Dondorp, Z. Bozdech, Peeling the onion: how complex is the artemisinin resistance genetic trait of malaria parasites?, Trends in Parasitology 40 (2024) 970–986. https://doi.org/10.1016/j.pt.2024.09.002.

[40] S. Yu, Hemoglobin: Physiology and Hemoglobinopathy, in: H. Liu, A.D. Kaye, J.S. Jahr (Eds.), Blood Substitutes and Oxygen Biotherapeutics, Springer International Publishing, Cham, 2022: pp. 45–51. https://doi.org/10.1007/978-3-030-95975-3_4.

[41] M.H. Rosove, Hemoglobin and Red Blood Cells Versus Malaria, in: M.H. Rosove (Ed.), Life's Blood: The Story of Hemoglobin, Springer Nature Switzerland, Cham, 2024: pp. 57–70. https://doi.org/10.1007/978-3-031-61150-6_7.

[42] J. Checa, J.M. Aran, Reactive oxygen species: Drivers of physiological and pathological processes, J. Inflamm. Res. 13 (2020) 1057–1073. https://doi.org/10.2147/JIR.S275595.

[43] M. Vasquez, M. Zuniga, A. Rodriguez, Oxidative Stress and Pathogenesis in Malaria, Frontiers in Cellular and Infection Microbiology 11 (2021).

https://www.frontiersin.org/journals/cellular-and-infection-microbiology/articles/10.3389/fcimb.2021.768182.

[44] Vani Rajashekaraiah, Masannagari Pallavi, Aastha Choudhary, Chaitra Bhat, Prerana Banerjee, Ranjithvishal, Shruthi Laavanyaa, Sudharshan Nithindran, Reactive Oxygen Species and Antioxidant Interactions in Erythrocytes, in: Vani Rajashekaraiah (Ed.), The Erythrocyte, IntechOpen, Rijeka, 2022: p. Ch. 1. https://doi.org/10.5772/intechopen.107544.

[45] M.N. Möller, F. Orrico, S.F. Villar, A.C. López, N. Silva, M. Donzé, L. Thomson, A. Denicola, Oxidants and Antioxidants in the Redox Biochemistry of Human Red Blood Cells, ACS Omega 8 (2023) 147–168. https://doi.org/10.1021/acsomega.2c06768.

[46] M. Depond, B. Henry, P. Buffet, P.A. Ndour, Methods to Investigate the Deformability of RBC During Malaria, Frontiers in Physiology 10 (2020). https://www.frontiersin.org/journals/physiology/articles/10.3389/fphys.2019.01613.

[47] S. Peslak, F. Sayani, 6 - Hemoglobinopathies and Thalassemias, in: R.E. Pyeritz, B.R. Korf, W.W. Grody (Eds.), Emery and Rimoin's Principles and Practice of Medical Genetics and Genomics (Seventh Edition), Academic Press, 2023: pp. 143–172. https://doi.org/10.1016/B978-0-12-812534-2.00009-6.

[48] M. Chauvet, C. Chhuon, J. Lipecka, S. Dechavanne, C. Dechavanne, M. Lohezic, M. Ortalli, D. Pineau, J.-A. Ribeil, S. Manceau, C. Le Van Kim, A.J.F. Luty, F. Migot-Nabias, S. Azouzi, I.C. Guerrera, A. Merckx, Sickle Cell Trait Modulates the Proteome and Phosphoproteome of Plasmodium falciparum-Infected Erythrocytes, Frontiers in Cellular and Infection Microbiology 11 (2021). https://www.frontiersin.org/journals/cellular-and-infection-microbiology/articles/10.3389/fcimb.2021.637604.

[49] H. Cao, M.A. Vickers, Oxidative stress, malaria, sickle cell disease, and innate immunity, Trends in Immunology 42 (2021) 849–851. https://doi.org/10.1016/j.it.2021.08.008.

[50] L. Luzzatto, M. Ally, R. Notaro, Glucose-6-phosphate dehydrogenase deficiency, Blood 136 (2020) 1225–1240. https://doi.org/10.1182/blood.2019000944.

[51] J.L. Parker, J.C. Deme, D. Kolokouris, G. Kuteyi, P.C. Biggin, S.M. Lea, S. Newstead, Molecular basis for redox control by the human cystine/glutamate antiporter system xc−, Nature Communications 12 (2021) 7147. https://doi.org/10.1038/s41467-021-27414-1.

[52] F.-J. Li, H.-Z. Long, Z.-W. Zhou, H.-Y. Luo, S.-G. Xu, L.-C. Gao, System Xc−/GSH/GPX4 axis: An important antioxidant system for the ferroptosis in drug-resistant solid tumor therapy, Frontiers in Pharmacology 13 (2022). https://www.frontiersin.org/journals/pharmacology/articles/10.3389/fphar.2022.910292.

[53] T.D. Hang, H.M. Hung, P. Beckers, N. Desmet, M. Lamrani, A. Massie, E. Hermans, K. Vanommeslaeghe, Structural investigation of human cystine/glutamate antiporter system xc− (Sxc−) using homology modeling and molecular dynamics, Frontiers in Molecular Biosciences 9 (2022). https://www.frontiersin.org/journals/molecular-biosciences/articles/10.3389/fmolb.2022.1064199.

[54] M. Nehser, J. Dark, D. Schweitzer, M. Campbell, J. Zwicker, D.M. Hitt, H. Little, A. Diaz-Correa, D.C. Holley, S.A. Patel, C.M. Thompson, R.J. Bridges, System Xc−Antiporter Inhibitors: Azo-Linked Amino-Naphthyl-Sulfonate Analogues of Sulfasalazine, Neurochemical Research 45 (2020) 1375–1386. https://doi.org/10.1007/s11064-019-02901-6.

[55] D. Patel, P.S. Kharkar, N.S. Gandhi, E. Kaur, S. Dutt, M. Nandave, Novel analogs of sulfasalazine as system xc− antiporter inhibitors: Insights from the molecular modeling studies, Drug Development Research 80 (2019) 758–777. https://doi.org/10.1002/ddr.21557.

[56] K. Okamoto, Y. Saito, H. Ueda, K. Narumi, A. Furugen, M. Kobayashi, Kinetic analysis of cystine uptake and inhibition pattern of sulfasalazine in A549 cells, Biopharmaceutics & Drug Disposition 42 (2021) 389–392. https://doi.org/10.1002/bdd.2298.

[57] L.M. Koehn, ABC Transporters: Multidrug Resistance-Associated Proteins, in: A. Talevi (Ed.), The ADME Encyclopedia: A Comprehensive Guide on Biopharmacy and Pharmacokinetics, Springer International Publishing, Cham, 2022: pp. 25–32. https://doi.org/10.1007/978-3-030-84860-6_79.

[58] G. You, M.E. Morris, Drug transporters : molecular characterization and role in drug disposition, Third edition, John Wiley & Sons, Inc., Hoboken, NJ, 2022. https://doi.org/10.1002/9781119739883.

[59] Y. Zhu, X. Xing, F. Wang, L. Chen, C. Zhong, X. Lu, Z. Yu, Y. Yang, Y. Yao, Q. Song, S. Han, Z. Liu, P. Zhang, The ATP-bound inward-open conformation of ABCC4 reveals asymmetric ATP binding for substrate transport, FEBS Letters 598 (2024) 1967–1980. https://doi.org/10.1002/1873-3468.14955.

[60] R. Nasr, D. Lorendeau, R. Khonkarn, L. Dury, B. Pérès, A. Boumendjel, J.-C. Cortay, P. Falson, V. Chaptal, H. Baubichon-Cortay, Molecular analysis of the massive GSH transport mechanism mediated by the human Multidrug Resistant Protein 1/ABCC1, Scientific Reports 10 (2020) 7616. https://doi.org/10.1038/s41598-020-64400-x.

[61] M. Wiese, S.M. Stefan, The A-B-C of small-molecule ABC transport protein modulators: From inhibition to activation—a case study of multidrug resistance-associated protein 1 (ABCC1), Medicinal Research Reviews 39 (2019) 2031–2081. https://doi.org/10.1002/med.21573.

[62] O. Fallatah, E. Georges, Apigenin-induced ABCC1-mediated efflux of glutathione from mature erythrocytes inhibits the proliferation of Plasmodium falciparum, International Journal of Antimicrobial Agents 50 (2017) 673–677. https://doi.org/10.1016/j.ijantimicag.2017.08.014.

[63] K.J. Wicht, S. Mok, D.A. Fidock, Molecular Mechanisms of Drug Resistance in Plasmodium falciparum Malaria, Annual Review of Microbiology 74 (2020) 431–454. https://doi.org/10.1146/annurev-micro-020518-115546.

[64] P. Tang, H. Wang, Regulation of erythropoiesis: emerging concepts and therapeutic implications, Hematology 28 (2023) 2250645. https://doi.org/10.1080/16078454.2023.2250645.

[65] A. Tkachenko, A. Onishchenko, Casein kinase 1α mediates eryptosis: a review, Apoptosis 28 (2023) 1–19. https://doi.org/10.1007/s10495-022-01776-3.

[66] T. Liu, B. Xiao, F. Xiang, J. Tan, Z. Chen, X. Zhang, C. Wu, Z. Mao, G. Luo, X. Chen, J. Deng, Ultrasmall copper-based nanoparticles for reactive oxygen species scavenging and alleviation of inflammation related diseases, Nature Communications 11 (2020) 2788. https://doi.org/10.1038/s41467-020-16544-7.

[67] M.J. Ridder, S.M. Daly, P.R. Hall, J.L. Bose, Quantitative Hemolysis Assays, in: K.C. Rice (Ed.), Staphylococcus Aureus: Methods and Protocols, Springer US, New York, NY, 2021: pp. 25–30. https://doi.org/10.1007/978-1-0716-1550-8_4.

[68] W. Trager, J.B. Jensen, Human Malaria Parasites in Continuous Culture, Science 193 (1976) 673–675. https://doi.org/10.1126/science.781840.

[69] M. Roncalés, J. Vidal, P.A. Torres, E. Herreros, In vitro culture of Plasmodium falciparum: obtention of synchronous asexual erythrocytic stages, Open Journal of Epidemiology 5 (2015) 71–80.

[70] Smilkstein Martin, Sriwilaijaroen Nongluk, Kelly Jane Xu, Wilairat Prapon, Riscoe Michael, Simple and Inexpensive Fluorescence-Based Technique for High-Throughput Antimalarial Drug Screening, Antimicrobial Agents and Chemotherapy 48 (2004) 1803–1806. https://doi.org/10.1128/aac.48.5.1803-1806.2004.

[71] K. Moll, A. Kaneko, A. Sherf, M. Wahlgren, Methods in malaria research, 6th ed., BEI Resources, 2013. https://www.beiresources.org/portals/2/MR4/Methods_In_Malaria_Research-6th_edition.pdf

[72] P.V. Dludla, B.B. Nkambule, S.E. Mazibuko-Mbeje, T.M. Nyambuya, S. Silvestri, P. Orlando, V. Mxinwa, J. Louw, L. Tiano, Chapter 25 - The impact of dimethyl sulfoxide on oxidative stress and cytotoxicity in various experimental models, in: V.B. Patel, V.R. Preedy (Eds.), Toxicology, Academic Press, 2021: pp. 243–261. https://doi.org/10.1016/B978-0-12-819092-0.00025-X.

[73] B. Gironi, Z. Kahveci, B. McGill, B.-D. Lechner, S. Pagliara, J. Metz, A. Morresi, F. Palombo, P. Sassi, P.G. Petrov, Effect of DMSO on the Mechanical and Structural Properties of Model and Biological Membranes, Biophysical Journal 119 (2020) 274–286. https://doi.org/10.1016/j.bpj.2020.05.037.

[74] C. Boulet, T.L. Gaynor, T.G. Carvalho, Eryptosis and Malaria: New Experimental Guidelines and Re-Evaluation of the Antimalarial Potential of Eryptosis Inducers, Frontiers in Cellular and Infection Microbiology 11 (2021). https://www.frontiersin.org/journals/cellular-and-infection-microbiology/articles/10.3389/fcimb.2021.630812.

[75] Z. Zheng, G. Luo, X. Shi, Y. Long, W. Shen, Z. Li, X. Zhang, The Xc− inhibitor sulfasalazine improves the anti-cancer effect of pharmacological vitamin C in prostate cancer cells via a glutathione-dependent mechanism, Cellular Oncology 43 (2020) 95–106. https://doi.org/10.1007/s13402-019-00474-8.

[76] A. Sugiyama, T. Ohta, M. Obata, K. Takahashi, M. Seino, S. Nagase, xCT inhibitor sulfasalazine depletes paclitaxel-resistant tumor cells through ferroptosis in uterine serous carcinoma, Oncol Lett 20 (2020) 2689–2700. https://doi.org/10.3892/ol.2020.11813.

[77] J. Liu, C. Lou, C. Zhen, Y. Wang, P. Shang, H. Lv, Iron plays a role in sulfasalazine-induced ferroptosis with autophagic flux blockage in K7M2 osteosarcoma cells, Metallomics 14 (2022) mfac027. https://doi.org/10.1093/mtomcs/mfac027.

[78] L. Yin, Z. Li, J. Wang, L. Wang, L. Hou, S. Hu, H. Chen, P. Luo, X. Cui, J. Zhu, Sulfasalazine inhibits esophageal cancer cell proliferation by mediating ferroptosis, Chemical Biology & Drug Design 102 (2023) 730–737. https://doi.org/10.1111/cbdd.14281.

[79] R. Joshi, S. Kumar, M. Unnikrishnan, T. Mukherjee, Free radical scavenging reactions of sulfasalazine, 5-aminosalicylic acid and sulfapyridine: Mechanistic aspects and antioxidant activity, Free Radical Research 39 (2005) 1163–1172. https://doi.org/10.1080/10715760500177880.

[80] M.I. Sonmez, A. Shahzadi, C. Kose, H. Sonmez, S. Ozyazgan, A.G. Akkan, Effect of sulfasalazine on endothelium-dependent vascular response by the activation of Nrf2 signalling pathway, Frontiers in Pharmacology 13 (2022). https://www.frontiersin.org/journals/pharmacology/articles/10.3389/fphar.2022.979300.

[81] S. Lin, H. Zhao, C. Xu, P. Zhang, X. Mei, D. Jiang, Sulfasalazine-loaded nanoparticles for efficient inflammatory bowel disease therapy via ROS-scavenging strategy, Materials & Design 225 (2023) 111465. https://doi.org/10.1016/j.matdes.2022.111465.

[82] F. Orrico, S. Laurance, A.C. Lopez, S.D. Lefevre, L. Thomson, M.N. Möller, M.A. Ostuni, Oxidative Stress in Healthy and Pathological Red Blood Cells, Biomolecules 13 (2023). https://doi.org/10.3390/biom13081262.

[83] P. Kashyap, D. Shikha, M. Thakur, A. Aneja, Functionality of apigenin as a potent antioxidant with emphasis on bioavailability, metabolism, action mechanism and in vitro and in vivo studies: A review, Journal of Food Biochemistry 46 (2022) e13950. https://doi.org/10.1111/jfbc.13950.

[84] J. Jodynis-Liebert, M. Kujawska, Biphasic Dose-Response Induced by Phytochemicals: Experimental Evidence, Journal of Clinical Medicine 9 (2020). https://doi.org/10.3390/jcm9030718.

[85] E.J. Calabrese, E. Agathokleous, R. Kapoor, G. Dhawan, V. Calabrese, Luteolin and hormesis, Mechanisms of Ageing and Development 199 (2021) 111559. https://doi.org/10.1016/j.mad.2021.111559.

[86] A. Tkachenko, O. Havranek, Erythronecroptosis: an overview of necroptosis or programmed necrosis in red blood cells, Molecular and Cellular Biochemistry 479 (2024) 3273–3291. https://doi.org/10.1007/s11010-024-04948-8.

[87] P. Bigdelou, A.M. Farnoud, Induction of Eryptosis in Red Blood Cells Using a Calcium Ionophore, JoVE (2020) e60659. https://doi.org/10.3791/60659.

[88] J.S. McCarthy, R.N. Price, 40 - Antimalarial Drugs, in: J.E. Bennett, R. Dolin, M.J. Blaser (Eds.), Mandell, Douglas, and Bennett's Principles and Practice of Infectious Diseases (Eighth Edition), W.B. Saunders, Philadelphia, 2015: pp. 495-509.e5. https://doi.org/10.1016/B978-1-4557-4801-3.00040-0.

[89] P. Koppula, L. Zhuang, B. Gan, Cystine transporter SLC7A11/xCT in cancer: ferroptosis, nutrient dependency, and cancer therapy, Protein & Cell 12 (2021) 599–620. https://doi.org/10.1007/s13238-020-00789-5.

[90] K. Devine, E. Villalobos, C.J. Kyle, R. Andrew, R.M. Reynolds, R.H. Stimson, M. Nixon, B.R. Walker, The ATP-binding cassette proteins ABCB1 and ABCC1 as modulators of glucocorticoid action, Nature Reviews Endocrinology 19 (2023) 112–124. https://doi.org/10.1038/s41574-022-00745-9.